SKB

# TECHNICAL REPORT 87-11

## Modelling of crustal rock mechanics for radioactive waste storage in Fennoscandia– Problem definition

Ove Stephansson
University of Luleå

May 1987

**SVENSK KÄRNBRÄNSLEHANTERING AB**
*SWEDISH NUCLEAR FUEL AND WASTE MANAGEMENT CO*

BOX 5864 S-102 48 STOCKHOLM
TEL 08-665 28 00 TELEX 13108-SKB

# MODELLING OF CRUSTAL ROCK MECHANICS FOR RADIOACTIVE WASTE STORAGE IN FENNOSCANDIA - PROBLEM DEFINITION

Ove Stephansson

University of Luleå

May 1987

# MODELLING OF CRUSTAL ROCK MECHANICS FOR RADIOACTIVE WASTE STORAGE IN FENNOSCANDIA - PROBLEM DEFINITION

Ove Stephansson

Maj 1987

SUMMARY

The problem of long term stability and geodynamic processes of the Baltic Shield has been adressed in the research plan for the coming six years, 1987-1992, of the Swedish Nuclear Fuel and Waste Management Company. The aims of the research activities are to quantify and place limits on the effects of earthquakes, glaciation and glacial rebound. Special attention will be paid to the safety analysis of a final storage of spent nuclear fuel.

In modelling the deformation of large scale rock masses and the stability of vaults for radioactive waste disposal, we need to know the geometry and structure of the geomechanical parameters of large rock masses and the boundary conditions that we might apply to our models.

Existing knowledge on crustal stresses and their orientation for Western Europe and North America is reviewed, and data on crustal stress gradients for Fennoscandia are presented. The vertical stress is taken to be equal to the weight of the overburden and the horizontal stress gradients are in accordance with shallow stress measurements, predominantly thrust fault earthquake fault plane solutions and ridge push at the Mid Atlantic Ridge as a major stress generating mechanism for the maximum horizontal stress.

Generic, two-dimensional models are proposed for vertical and planar sections of a traverse having a direction NW-SE in Northern Fennoscandia. The vertical section comprises a three-layered model of the lithosphere from the oceanic-continental crustal boundary at the shelf of the North Sea, to the centre of uplift in the Bothnian Bay. Faults are assumed to extend down to the upper-lower crust boundary at a depth of about 20 km. The proposed traverse will include the major neotectonic structures at Lansjärv and Pärvie, respectively, and also the study site for storage of spent nuclear fuel at Kamlunge, close to the SE end of the traverse.

In modelling the influence of glaciation, deglaciation and glacial rebound on crustal rock mechanics and stability, two modelling ap-

proaches are suggested. In the first approach, the ground surface and the crustal-mantle interface has a prescribed shape in accordance with known functions of elastic-viscous rebound for each side of the ice front and the uplift is varied according to existing knowledge about total, present and remaining uplift.

The second modelling approach uses ice as a surface load, where the boundary of the ice sheet follows the extension of the Weichselian glacial ice at the continental shelf of Northwestern Norway.

In principal three different size of models are suggested. Global models, with a length of about 100 km, will make it possible to increase our overall understanding of the change in stresses and deformations and they can provide boundary conditions for regional and near-field models, cf. Fig. 4.6. The regional models can be used for studies of the neotectonic structures and the near-field models will be used for stability analysis of the vault for final storage of spent nuclear fuel.

The last section of the report is devoted to a study of the strength of granitic rock masses. Here the rock mass discontinuity characteristics are shown to be of equal, or even greater importance in studies of crustal stability and integrity of vaults than is the case with much stronger and stiffer intact rocks. Differences in the shear strength of rock joints and faults at low and high effective normal stress are demonstrated and equations to describe these properties are presented. The stiffness of joints and faults is assumed to be independent of the block size, whereas shear stiffness is most likely to vary as a function of the length of the joint/fault and the effective normal stress. Properties of this type must be considered in the modelling of the crustal rock mechanics for any of the three models described above.

CONTENTS

ABSTRACT

In modelling the deformation of large scale rock masses and the stability of vaults for radioactive waste disposal, we need to know the geometry and structure of large rock masses and the boundary conditions that we might apply to our models.

Existing knowledge of crustal stresses for Fennoscandia is presented. Generic, two-dimensional models are proposed for vertical and planar sections of a traverse having a direction NW-SE in Northern Fennoscandia. The proposed traverse will include the major neotectonic structures at Lansjärv and Pärvie, respectively, and also the study site for storage of spent nuclear fuel at Kamlunge. The influence of glaciation, deglaciation, glacial rebound on crustal rock mechanics and stability is studied for the modelling work.

Global models, with a length of roughly 100 km, will increase our over all understanding of the change in stresses and deformations. These can provide boundary conditions for regional and near-field models.

The final section of this report is devoted to a study of the strength of granitic rock masses. Properties of strength and stiffness of intact rocks, faults and joints must be considered in the modelling of the crustal rock mechanics for any of the three models described above.

# 1 INTRODUCTION

An understanding of the stability of the bedrock of Fennoscandia is of outmost importance to existing ideas on the question of the final stor age of spent nuclear fuel in granitic rocks. The problem of longterm stability of the crust has been adressed in the research plan for the coming six years, 1987-1992, of the Swedish Nuclear Fuel and Waste Management Company, (1986). As a part of the research program, long term rock stability modelling of the response of rock masses to external loads from earthquakes, glaciation and glacial rebound will be conducted. The neotectonics at Lansjärv, Northern Sweden, will be studied in detail. Before any modelling is undertaken, we must know the type and behaviour of the external loads. The aim of this study is therefore to present the crustal stresses and their orientation and gradients in Fennoscandia,the strength of granitic rock masses in the crust, erosion, glaciation and land uplift.

When any potential bedrock site located in the Fennoscandian Shield is examined, we are confronted with a very complex geological history embodying several stages of extreme tectonic disturbance that have distorted, fractured and faulted and otherwise transformed the rocks from the state in which they were originally formed. At a first glance, the prediction and modelling of the present and future stability of these rocks appears to be a very complex problem. However, there are two reasons for optimism. First, the Shield has been tectonically quiescent over a very long period of time. Paleomagnetic and radiometric results prove that the Shield has been intact over the last 1.8 Ga including late crustal accretion, Pesonen and Neuvonen (1981). Thus, the loading, deformation and uplift that accompanied cycles of Quaternary glaciation were by far the strongest events of the last 10 Ma. It is not therefore surprising that a variety of faults, fractures, and some earthquake activity has been produced for shield areas, West (1984), Talbot (1986).

In a discussion on past geological conditions and their relevance to present-day fracture flow systems, Brown et al. (1983) reached the conclusion that the response of the Archean fracture system in Western

Ontario, Canada, to variations in geologic conditions through time appears to be largely confined to a repeated reactivation, and possibly of the existing fracture network alone. This suggests that the effects of any future event will also be largely restricted to a reactivation of parts of the existing network.

A repository for radioactive waste must be located and designed to be protected against (i) natural changes of first order (faulting, glaciation, meteorite impact) (ii) human activity (war, sabotage, mining) (iii) degradation of engineering and natural barriers (corrosion of canisters, penetration of bentonite buffer, ground-water transport). To protect the repository from first order faulting, Stephansson et al. (1978) suggested its location in a large block of a jointed rock mass surrounded by faults or shear zones. Any large scale movements will then appear along pre-existing faults and the repository in the centre of the large block will be protected. Later Stephansson (1983) presented mathematical models of a repository and deposition holes to prove the stability of the underground constructions. In modelling large scale rock masses and the farfield stability of vaults for radioactive waste disposal, we are faced with new problems. Here there are a limited number of studies in which cubic kilometres of rock masses are simulated. One example is the modelling of compaction and subsidence of the Ekofisk oil and gas field in the North Sea (Barton et al., 1986).

Since we intend to model the crustal rock mechanics, we must know the geometry and structure of the geomechanical parameters of large rock masses and the boundary conditions which might be applied to our models. In Chapter 2, existing knowledge on the state of stress in the earth crust is reviewed and the boundary stresses of a three-layer model of the crust and upper mantle is presented. Chapter 3 gives a description and a generic model of Fennoscandian fault structures and also the motivation for studying a geological traverse from the northernmost part of the Gulf of Bothnia in a nortwesterly direction to the area of Senja at the Norwegian shelf. Glaciological aspects of waste disposal are presented in Chapter 4 and a number of possible models for analysis are presented. Strength of intact rocks, discontinuities and rock masses are presented in Chapter 5. Based on the

existing knowledge of the mechanical properties of the crust and upper mantle presented in this report, we are able to make the necessary idealization of the problem to be studied and also select the of numerical models to be used.

# 2 CRUSTAL STRESSES AND THEIR ORIENTATIONS

An understanding of the in-situ state of stress within the Earth's crust is a vital requirement for the study of rock mass stability related to the disposal of nuclear fuel waste in rocks. We must know the stress field in order to study the rock mechanical effects and rock mass stability of future glaciations and deglaciations on a disposal vault. This is true in the study of both the nearfield and farfield rock mechanics of the vault. The aim of this section is therefore to present the most likely stress gradients and stress orientations for the Fennoscandian Shield.

## 2.1 Change of stresses with depth

Many compilations of in-situ stress measurements, made in various parts of the world, have now been published. The most recent collection of data on the state of stress in the earth crust is presented in the proceedings of the International Symposium on Rock Stress and Rock Stress Measurements held in Stockholm, 1-3 September 1986 and edited by Stephansson (1986). Of special interest to this study are the contributions by Stephansson et al. (1986), Klein and Barr (1986), and Herget (1986).

Stephansson et al. (1986) presented some preliminary results from the established Fennoscandian Rock Stress Data Base (FRSDB) which, at present, contains almost 500 entries from 102 sites in Finland, Norway and Sweden. Regression analyses of maximum and minimum horizontal stresses versus depth for four different stress measurement methods were presented. These are shown in Figure 2.1. From the compiled data in FRSDB we can draw the following conclusions on changes of stress with depth:

- there is a large horizontal stress component for the uppermost 1000 m, which may be due to a combination of remanent stresses from the previous tectonic orogenies, plate tectonic stresses and glacial related stresses

- discrepancies in the variations in magnitude of stresses with depth have been obtained when different rock stress measurement methods are used. Of all the methods used, the overcoring method of Hast gives by far the largest stress gradients and intercepts of stress at the ground surface, cf. Figure 2.1

- for all methods it was found that maximum and minimum horizontal stress exceed the vertical stress as determined from the weight of the over burden

- stress measurements from the Leeman, Leeman-NTH, Leeman-LuT overcoring methods have revealed minor differences in the magnitudes of the minimum horizontal stress, $\sigma_{HMIN}$, and the vertical stress, $\sigma_V$. In regions where $\sigma_{HMIN}$ happens to be greater than $\sigma_V$, thrust faulting will appear once the rock mass strength is exceeded. In others, where $\sigma_{HMIN}$ is less than $\sigma_V$, strike slip faulting will occur.

- regression analyses of the principal stresses versus depth for the overcoring rock stress measurement methods give the following results:

$$\sigma_1 = 0.050 \cdot z + 7.9 \quad , \quad r = 0.61$$

$$\sigma_2 = 0.32 \cdot z + 4.2 \quad , \quad r = 0.60$$

$$\sigma_3 = 0.019 \cdot z + 0.6 \quad , \quad r = 0.56$$

where z is the depth in meters and the stresses are expressed in MPa.

Because of the many similarities in the geology of the Canadian and Fennoscandian Shield, and in particular the late Quaternary geology, a closer look at the existing stress data from Canada is of value to this study. When data on stress gradients was first published in Canada, the data base was rather small and some of the results from ground stress measurements were of questionable quality. In a recent paper Herget (1986) provides an update of previously published compilations. Most of the sites are located in the Superior and Southern Tectonic Province of the Canadian Shield, which consist of Archean and

Proterozoic rocks. The data which has been compiled clearly shows that near the surface, horizontal stress components exceed the stress values derived from overburden load.

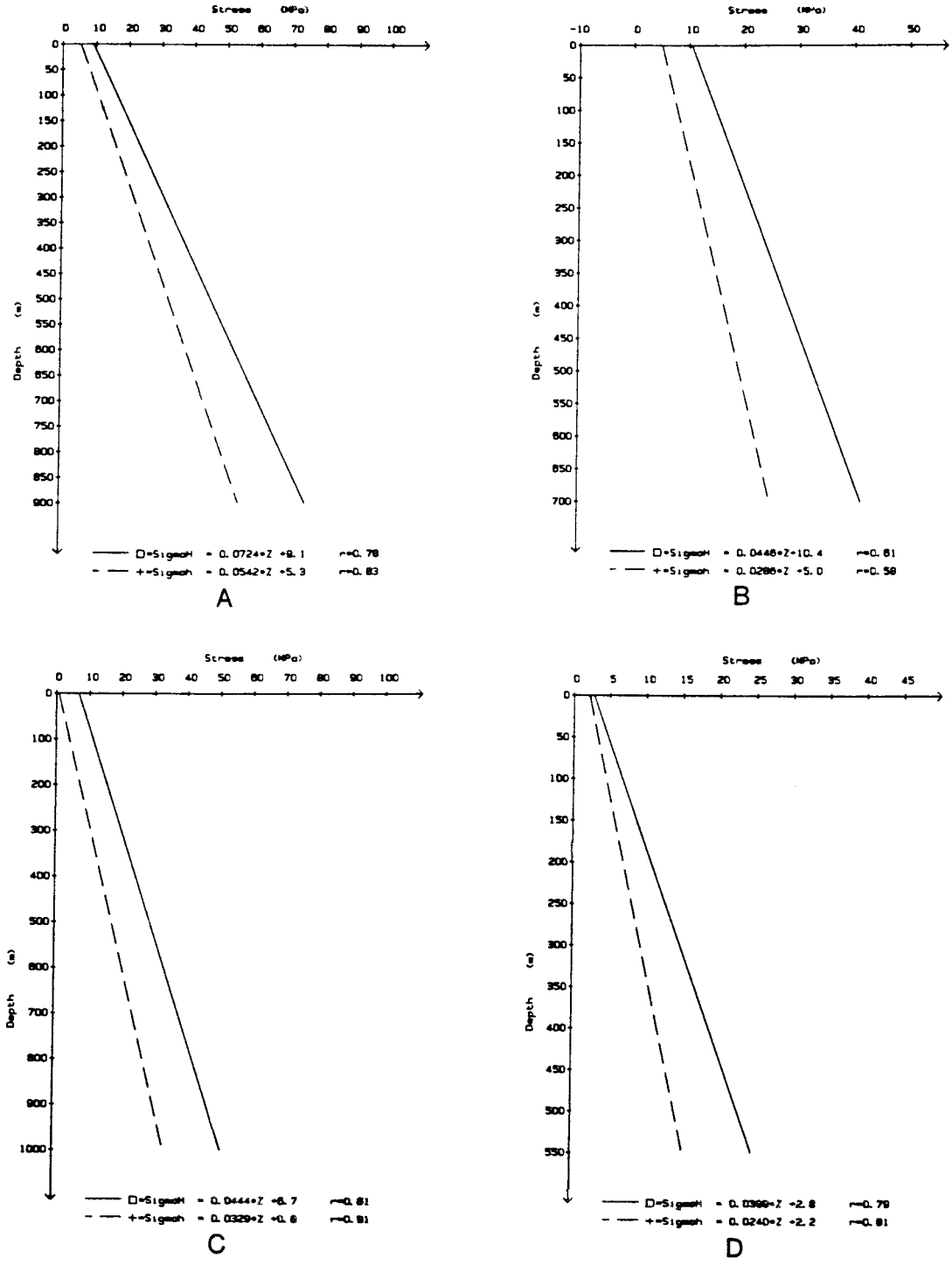


Fig. 2.1 Regression analyses of maximum horizontal stress ($\sigma_H$) and minimum horizontal stress ($\sigma_h$) versus depth for four different rock stress measurement methods. A) Hast overcoring; B) Leeman-Hiltscher, Swedish State Power Board, overcoring; C) Leeman, Leeman-NTH, Leeman-LUT, overcoring; and D) hydraulic fracturing, LBL, CTH and LUT. After Stephansson et al. (1986).

From the analysis of 54 ground stress tensors Herget (op. cit.) found that in the Canadian Shield there seems to be a "normal" and an extreme "population" in the stress data. For the so-called "normal population", the vertical stress components are close to the overburden load, whereas the extreme population shows vertical stresses far in excess of those derived from the overburden load.

The increase of the average horizontal stress with depth could be described by means of a bi-linear relationship for the two depth interval 0-800 m and 800-2000 m. For the extreme population Herget found a linear increase of the average horizontal stress with depth. The change of average horizontal stress and the change in ratio of the horizontal stress to the vertical stress with depth are shown in Figure 2.2. From the data compiled in Canada, we can draw the following conclusions on changes of stress with depth, and how this compares with the situation in Fennoscandia:

- there is a high horizontal stress component for the uppermost 800 m which may be due to a combination of remanent stresses from the previous tectonic orogenies, plate tectonic stresses and glacially related stresses. This situation is almost identical to that of the Fennoscandian Shield

- ground stress determinations in Canada were performed by overcoring methods using bi-, and tri-axial instruments. Hence, the data for Canada presented by Herget (op. cit.) should be compared with the results shown in Figures 2.1 A and B for Fennoscandia. We see here that the stress gradient for the average horizontal stress in the uppermost 800 m of the Canadian Shield is somewhat greater than the corresponding gradient in Fennoscandia

- for most of the stress measurements in Canada, the maximum and minimum horizontal stress exceed the vertical stress, cf. Figure 2.2 B. A similar situation is valid for the Fennoscandian Shield, and this was found to matter what measurement method was used

- a minor difference in magnitudes of the minimum horizontal stress ($\sigma_{HMIN}$) and the vertical stress for depths greater than 200 m is

found in the Canadian Shield. It appears that the same is true for the Fennoscandian Shield, and thrust faulting or strike slip faulting are equally likely to occur once the rock mass strength is exceeded

- according to Hasegawa et al. (1985) a lower limit to the deviatoric stress in the upper crust of eastern Canada can be inferred from the stress drop of earthquakes in the Canadian Shield, which tend to have an upper limit of about 10 MPa. A similar situation regarding stress drops in the Fennoscandian Shield has been suggested by Slunga et al. (1984).

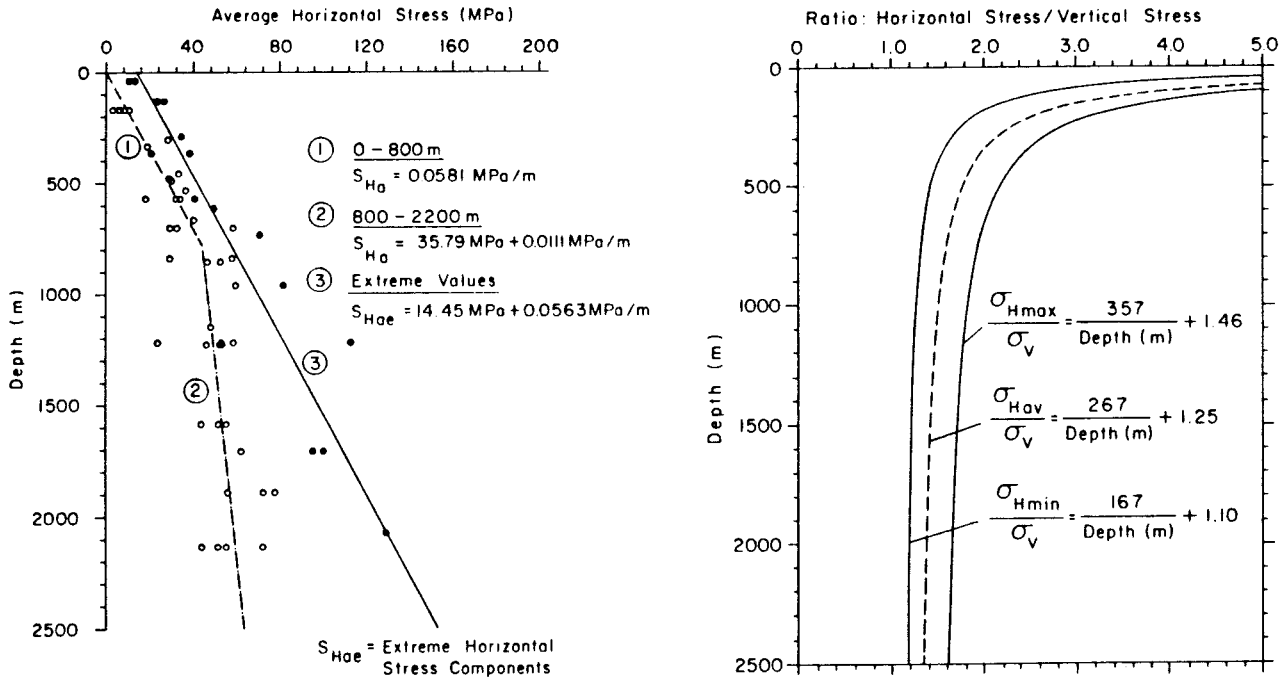


Fig. 2.2 State of stress in the Canadian Shield. A) Change of average horizontal stress components with depth; and B) Change of ratio of horizontal stress/vertical stress with depth. After Herget (1986).

In the discussion of stress gradients in the upper crust, we should note the major discontinuity in the stress field that has recently been reported from several test sites. Three out of four reported stress anomalies in this report are related to the Canadian and Fennoscandian Shield areas. Martna et al. (1983) reported stress anomalies of the order of 20 MPa for the maximum horizontal stress across a

major fracture zone at 320 m depth of a vertical borehole at Forsmark, Central Sweden. A similar situation was obtained from the stress measurements at Lavia, Central Finland (Bjarnason and Stephansson, 1987). A stress anomaly of about 20 MPa was inferred from measurements on each side of a major fracture zone at 420 m depth in Proterozoic granodiorite rocks.

The third example of a recorded stress anomaly is reported from hydrofracture stress determinations in borehole URL-1 of the Lac du Bonnet batholith, Manitoba, Canada, Haimson (1982). Just below the 320 m level, a major fracture zone caused a stress anomaly of about 10 MPa for the minimum horizontal stress and 25 MPa for the maximum horizontal stress. This stress anomaly was followed by a 90 degree rotation of the direction of the maximum horizontal stress. Finally, a stress anomaly of 28 MPa was recorded across a lithological boundary from 2490 to 3100 m in jointed granitic rocks near the Valles Caldera in New Mexico, Kelker et al. (1986).

At this stage of the study, we can conclude that stress anomalies across fracture zones and lithological boundaries have been recorded, that the stresses are reoriented and that the stress changes are of the order of a few tens of megapascals and of the same order of magnitude as the stress drops generated by shield earthquakes.

## 2.2 Orientation of stresses

In 1958, Hast published a compilation of in-situ rock stress measurements made in boreholes within the Fennoscandian Shield. Most of these measurements were conducted in mines and for several measuring sites in the near vicinity of mining operations.

In a later compilation which included Hast's data, Ranalli and Chandler (1975) concluded that within the southern part of the Fennoscandian Shield the maximum horizontal stress is directed approximately E-W while in the northern part of the Shield the trend is more N-S. This picture of the stress direction in Fennoscandia was maintained

until Slunga et al. (1984) published data from earthquake fault plane solutions of the southern parts of the Fennoscandian Shield. Their result is summarized as follows: The seismicity of the southern part of the Baltic shield has been studied for four years by a digital regional seismic network, with a station spacing of 100 km. Some 160 earthquakes have been analysed for location, focal depth, seismic moment, fault plane solution and static stress drop. More than 90 % of the earthquakes occur at depths less than 19 km. The orientation of the horizontal stresses relaxed by the events is very consistent, the principal compression is oriented in a NW-SE direction. The geographical distributions of the events show relations to the regional geology. The consistency of the stress pattern means that the type of faulting is determined mainly by the strikes of the available faults.

In a recent paper, Klein and Barr (1986) presented a compilation of previously published Western European in-situ stress data, together with results of wellbore breakout analyses of wells drilled in the North Sea, the Atlantic Ocean and onshore Britain. They found that within Central and Northern Europe, the North Sea, the Atlantic Ocean, the British Isles and Northern Scandinavia the regional direction of maximum horizontal stress is aligned approximately NW-SE, cf. Figure 2.3. In Southern Scandinavia they claim that the maximum stress direction to be approximately E-W. However, the data they present are based on old measurements and this statement is not valid. Klein and Barr (op. cit.) concluded that the consistent NW-SE orientation of the maximum horizontal in-situ stress direction over Western Europe is dominated largely by plate tectonic boundary forces acting upon the Eurasian tectonic plate. These forces include plate edge forces (for example com pressive ridge push forces perpendicular to the Eurasian/ African continental collision zone as expressed by the Alps).

A compilation and evaluation of the direction from the Fennoscandian Rock Stress Data Base is in progress. Preliminary results indicate larger scatter in the direction of the maximum principal horizontal stress than was obtained by Klein and Barr (1986) for Western Europe.

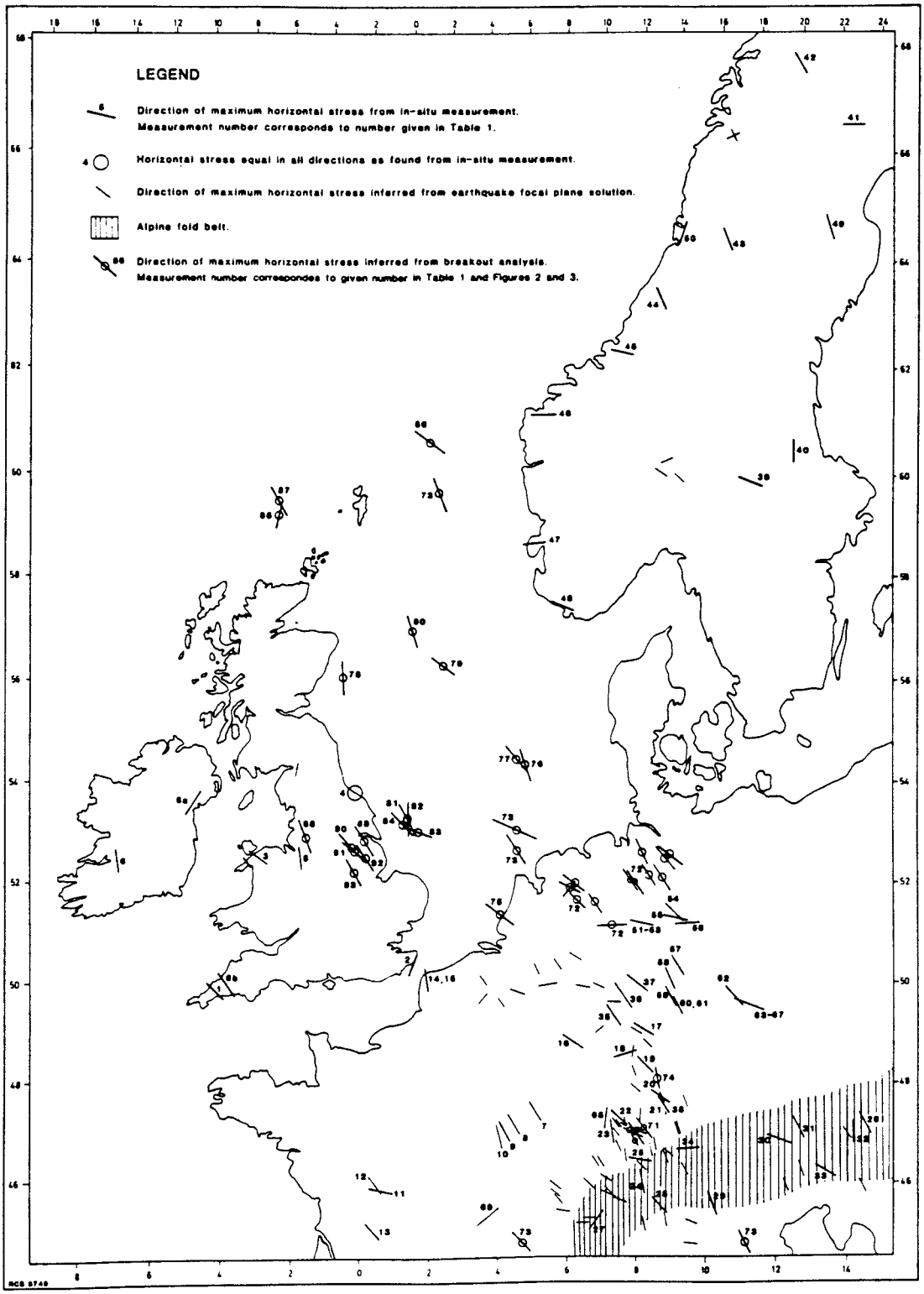


Fig. 2.3 Orientation of maximum horizontal principal stress within Western Europe. After Klein (1986).

A NW-SE direction for the maximum horizontal stress is strongly supported by evidence from fault plane solutions of earthquakes for Fennoscandia as presented by Slunga et al. (1984).

In the recent literature on the state of stress in the Earth's crust, several authors, e.g. Bott and Kusznir (1984) and Klein and Barr (1986), have suggested that the constant orientation of the maximum horizontal in-situ stress is governed by plate tectonic boundary forces. There is strong evidence to support this idea, e.g. for Western Europe. If this is correct, a study of the state of stress in the North American plate west of the Mid Atlantic Ridge to support the idea of deriving stresses from plate tectonic models further would be of great interest.

The orientation of deviatoric compressive stress in eastern Canada has been presented by Hasegawa et al. (1985). The data is derived either directly from in-situ stress measurements or is indirectly inferred from earthquake fault plane solutions, quarry floor buckles, pop-ups and postglacial faults. These data are summarized in Figure 2.4. The orientation of the maximum principal stress determined from near-surface stress measurements indicate, on average, an ENE direction, as does the orientation of quarry floor buckles. Postglacial thrust faults indicate a norherly direction of the stress field these faults are supposed to be related to deglaciation. They are not therefore necessarily indicative of the current stress field, cf. the stuctural analysis of the postglacial faults in Northern Sweden by Talbot (1986). From the diversified phenomena and data that contribute to existing knowledge of the stress field in eastern Canada, Hasegawa et al. (op. cit., p. 3639) draw the following conclusion: "Since near-surface stress indicators may be strongly affected by weathering, topography, and other near-surface features, the degree of correlation between near-surface stresses and the underlying stress field (> 300 m) is still uncertain. Nevertheless, there appears to be an overprint in the NE direction."

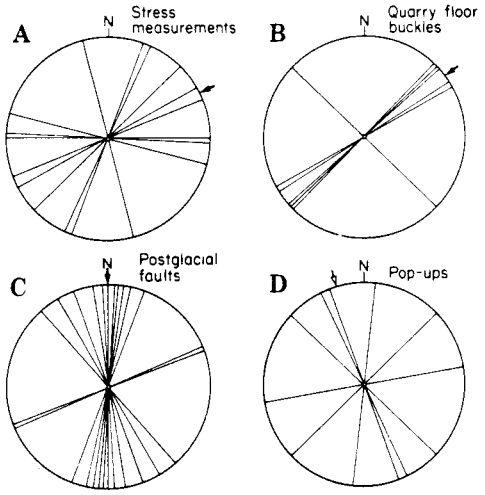


Fig. 2.4 Summarizied diagram showing azimuth of maximum horizontal stress directions inferred from measurements (< 300 m) and surficial fetures These are not stereograms. Solid arrows denote mean compression direction; open arrow denotes large uncertainty. After Hasegawa et al. (1985).

In a recent manuscript for the GSA Memoir in the Geophysical Framework of the Continental United States, Zoback and Zoback (1986) present an up-date of the classical Zobak and Zoback (1980) compilation of the stress orientation data for the continental (conterminous) United States. The data base has been enlarged from 226 points to more than 400 points. These data points have also been assigned a quality ranking. Stress orientations are obtained from three principal types of indicators: earth quake focal mechanisms, in-situ stress measurements and geological data on younger volcanics and fault offsets. Utilizing these data, they have prepared a map of maximum horizontal principal stress orientations. These are shown in Figure 2.5. The size of the arrow is scaled proportionally to its quality and the center symbol designates the type stress indicator; the maximum horizontal compressive stress orientation is plotted regardless of the actual stress state.

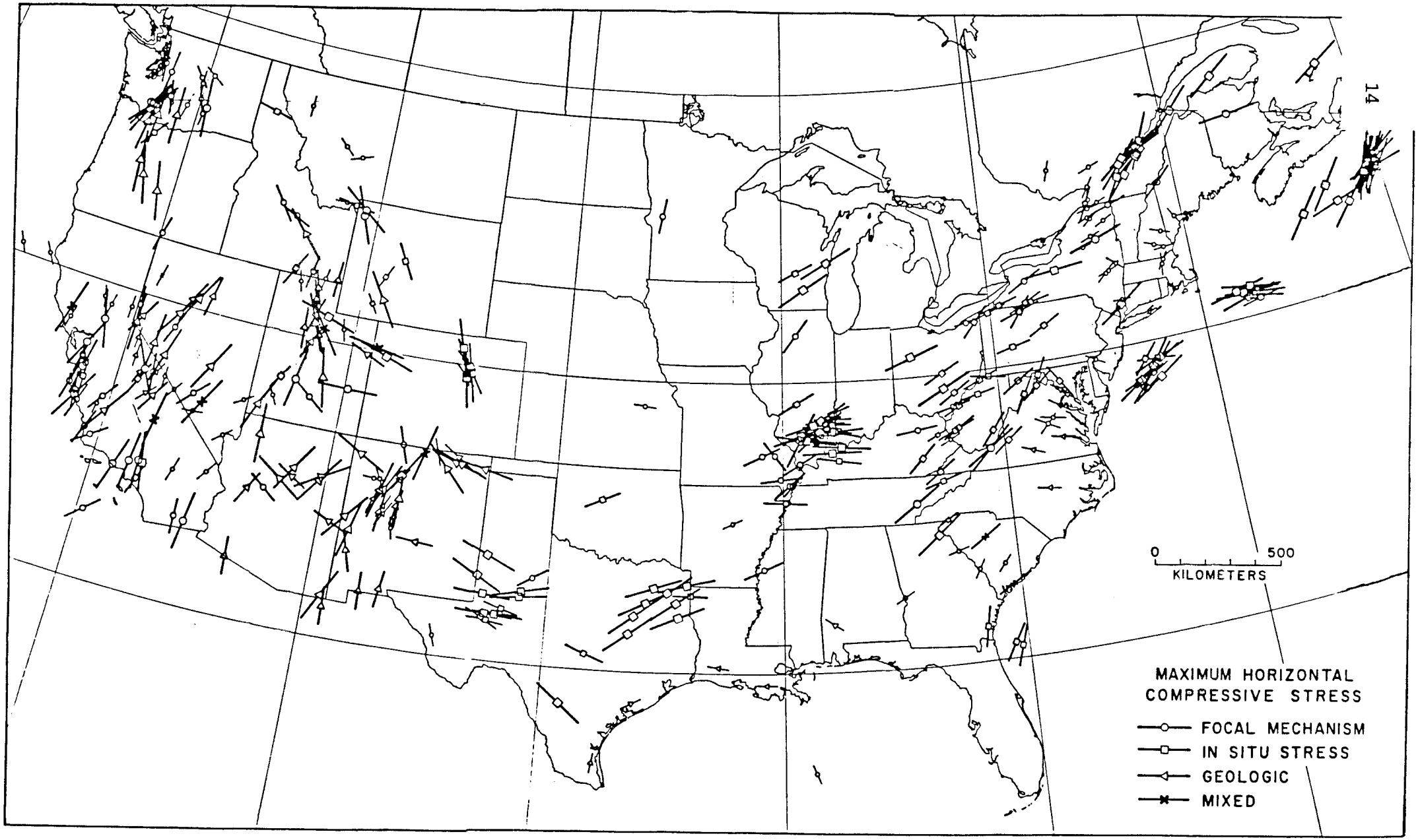


Fig. 2.5 Map of maximum horizontal compressive stress orientations. Quality of data indicated by weight and length of line. After Zoback and Zoback (1986).

From the data collected, Zoback and Zoback (1986) present a generalized stress map, Figure 2.6. This gives the average principal stress orientations, stress regimes and delineating stress provinces. From stress data and seismicity information, the stress provinces shown in Figure 2.6 are separated into four "plate-tectonic" provinces, namely: San Andreas transform, Rocky Mountain/Intermountain intraplate, Cascade convergent and the midplate central and eastern United States. Much of the midplate area is characterized by a compressive stress regime with reverse and strike-slip faulting and with vertical stresses less than one or both of the horizontal stresses. On the generalized stress map, we also notice that large portions of the western U.S. are currently undergoing extensional tectonism, i.e. the vertical stress is the maximum principal stress.

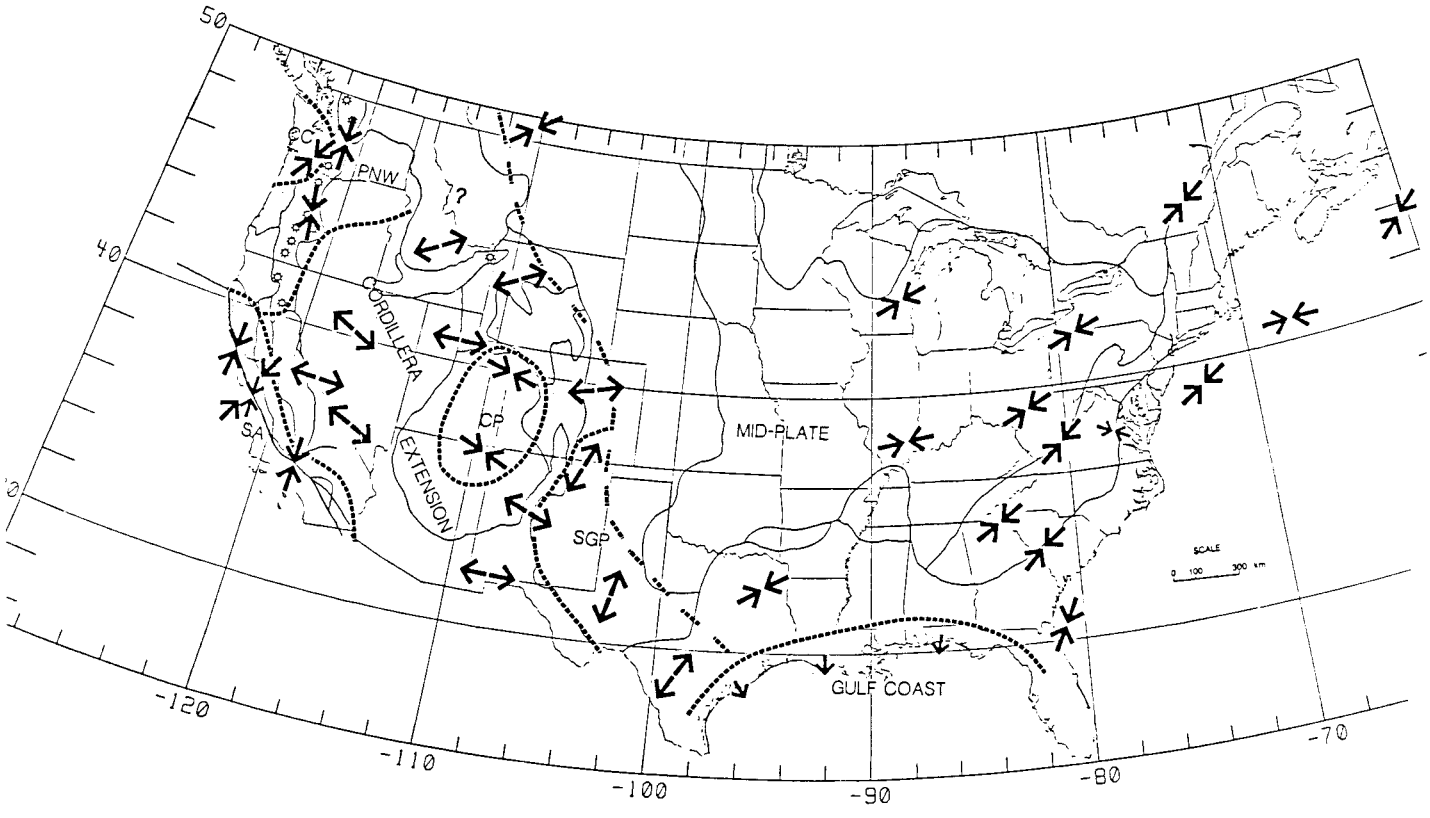


Fig. 2.6 Generalized stress map for the continental United States. Outward-pointing areas are given for areas characterized by extensional deformation. Inward-pointing areas are shown for regions dominated by compressional tectonism (thrust and strike-slip faulting). Stress provinces are delineated by the thick broken lines: CC - Cascade convergent province, PNW - Pacific Northwest, SA - San Andreas province, and CP - Colorado Plateau interior. After Zoback and Zoback (1986).

A large body of new data, and in particular well bore breakouts, have cast serious doubt on the existence of an Atlantic Coast stress province characterized by NW compression, as suggested by Zoback and Zoback (1980). Instead, stress orientations from the Great Plains east to the eastern United States and Canada appear to be generally consistent with a maximum horizontal stress orientation between NE and E (on average, roughly ENE). Based on a limit number of studies of focal mechanisms this compressive stress province is also assumed to be extended eastward throughout much of the western Atlantic basin.

Zoback and Zoback (1986) believe that the regional in-situ stress field is tectonic in origin and that the uniformity in the midplate stress pattern suggests a far-field source. Further, they make two general observations that lead them to prefer ridge push over basal drag as the primary source of stress in the midplate region. In an absolute reference frame, the North American cratonic continent is moving southwesterly and therefore drag-related compression should be most pronounced along the southwestern margin of the craton. However, a close look at Figure 2.6 demonstrates that this margin is characterized by an extensional stress régime in the Southern Great Plains. The second observation in favour of ridge push is the general increase in seismic activity from west to east within the craton. Hence, the overall uniformity in the midplate stress pattern suggests a far-field source. Since the North American Plate does not have any subducting slab, the most likely plate driving forces are ridge push and basal drag. At present, several arguments favour ridge push as the driving force of the plate and the compressive stress generating mechanism.

Summarizing the state of art about orientation of stresses on each side of the Mid Atlantic Ridge and far from the edge of the Eurasian and North American plate boundary we find the following:

- Western European in-situ stress data together with results of well-bore breakouts show that within Central and Northern Europe, the North Sea, the Atlantic Ocean and the British Isles, the regional direction of maximum horizontal stress is aligned approximately NW-SE

- data from earthquake fault plane solutions for the southern part of the Fennoscandian Shield indicates a very consistent NW-SE direction of the principal compression

- there is still some uncertainty in the degree of correlation in the direction and magnitudes between near surface stresses and the underlying stress field (> 300 m). This appears to be valid for data collected in eastern Canada and in Fennoscandia and is due to the effects of weathering, topography, glacial rebound, etc. on the near-field stress indicators

- recent compilation of stress orientation for eastern United States and Canada indicate a generally consistent maximum horizontal stress orientations between NE and E, and on average rougly ENE

- there is a strong belief that the regional in-situ stress field in Western Europe and eastern North America is tectonic in origin and that the uniformity in the stress pattern suggests a far-field source

- plate edge forces such as compressive ridge push forces perpendicular to the strike of the Mid Atlantic Ridge are believed to give rise to the consistent stress directions in the two plates.

## 2.3 Crustal stress gradients in Fennoscandia

The sources of lithospheric stresses and their distinctive features are subjects of the greatest interest in modern geophysics and tectonics, Salomon et al. (1980), Bott and Kusznir (1984), Hasegawa et al. (1985) and Zoback and Zoback (1986). In modelling the crustal rock mechanics due to glacial loading and rebound and postglacial instability like faulting, we should understand the principal categories of lithospheric stress. The lithosphere is the relatively strong outer layer of the Earth roughly 100 km in thickness which can support substantial deviatoric stresses. This property differs from the underlying asthenosphere and deeper parts of the Earth where the stress differences are relatively small, as a result of creep.

Stress systems affecting the lithosphere can be divided into two main categories which we refer to as renewable and non-renewable types (Bott and Kusznir, 1984).

Renewable stress systems are those which persist as a result of boundary or body forces even though the strain energy is progressively dissipated. Stresses arising from plate boundary forces and from isostatically compensated surface loads are the two main examples of relevance to the situation in the Fennoscandian Shield. The persistant plate boundary forces cause the plates to move relatively to each other. Geological evidence, thermodynamic considerations and comparison of observed stresses with predicted values all indicate that the plates are driven by boundary forces rather than by mantle drag. This means that the plate moves faster (i.e. of the order of a few centimeters per year for the Eurasian plate), than the underlying mantle. Mantle drag therefore opposes plate motion, rather than drive it. Bott and Kusznir (op. cit.) distinguish three principle types of driving forces

- ridge push force (compression, 20-30 MPa)
- slab pull force (tension, 0-50 MPa (?))
- trench suction force (tension, 0-30 MPa (?))

Examples of simple stress systems within lithospheric plates caused by plate boundary forces are shown in Figure 2.7. The most relevant model for the Fennoscandian continental crust of the Eurasian plate is given by examble b) in the figure. Ridge push forces at the Mid Atlantic Ridge and trench suction forces the Pacific cause stresses to change from compressive at ridge to tensile at trench. Later in this section we will analyse a recent model to determine the stress distribution in the lithosphere.

For renewable stress systems, the lithosphere acts as a reservoir of "strain energy reservoir" fed by the action of boundary or body forces, and relieved at approximately the same rate by tectonic activity. Loading of the lithosphere by surface topography, lateral density variation or ice sheets generates local stress fields. An elevated

region 1 km in height and of density 2.6 tons/$m^3$ would give rise to a stress difference of about 17 MPa. The deviatoric stresses that develop from ice loading will be discussed in Chapter 4.

Non-renewable stress systems are those which may be completly dissipated by release of the strain energy initially present. Bott and

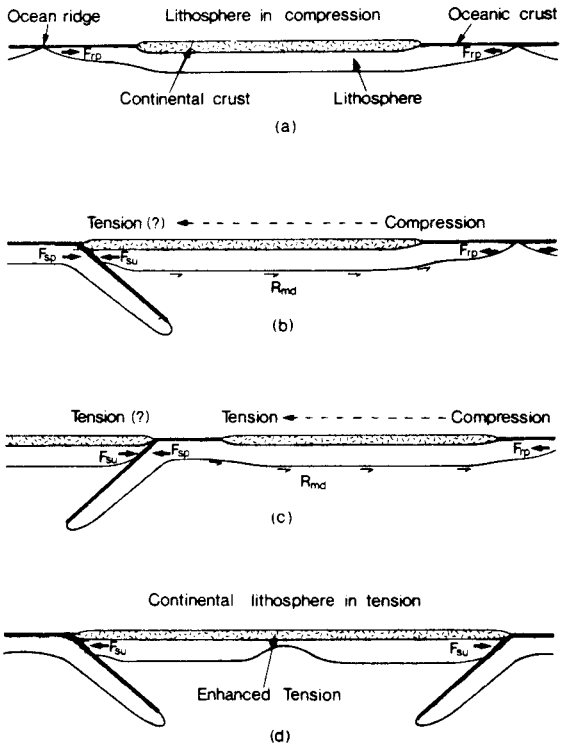


Fig. 2.7 Examples of simple stress systems within lithospheric plates generated by plate boundary forces. a) Ridge push force developed at ocean ridges on opposite sides of a plate, causing the whole plate to be in compression; example present African plate. b) Ridge push force on one side of a plate and trench suction force on opposite side, causing stress system changing from compressive at ridge to possibly tensile at trench (if local overriding plate resistance is high, compression may occur throughout the plate); example present South American plate. c) Ridge push force on one side of a plate and slab pull on opposite side, stress as in b); example Carboniferous basin formation in Great Britain. d) Trench suction on opposite sides of an entirely continental plate producing tension throughout; example Pangea just prior to its break-up.
$F_{rp}$ = ridge push; $F_{sp}$ = slab pull; $F_{su}$ = trench suction; $R_{md}$ = mantle drag.
After Bott and Kusznir (1984).

Kusznir (1984) list the following significant sources for non-renewable stress systems

- bending stresses at subduction zones
- membrane stresses caused by changes in radii of curvature of a plate as it migrates in latitude
- thermal stresses due to temperature changes in the lithosphere
- other mechanisms, e.g. phase transition, tidals ($10^{-3}$ MPa)

Of these stress generating systems, membrane stresses are thought to be the only stresses of importance in crustal rock mechanics modelling related to radioactive waste disposal in the Fennoscandian Shield.

Global stress models have been calculated for a variety of possible driving forces. One of the first examples of intraplate stress modelling by using a finite element technique was presented by Stephansson and Berner (1971). Based on the gravity model by Talwani, they modelled a section of the crust east of the Mid Atlantic Ridge. It was found here that most of the stresses were transmitted in the crust, and also that very low deviatoric stresses appeared in the mantle, cf. Figure 2.8.

Solomon et al. (1980) presented global intraplate stress models by using a finite element method in which the effect of wide variety of possible driving force combinations could be simulated. The best fitting global stress models include ridge pushing forces as an essential element. Like the modelling conducted by Stephansson and Berner (op. cit.), the horizontal stress at the ridge was exerted by the ridge elevation. In one possible global model that provides reasonably good fit with most of the intraplate stress orientation data, the following forces are included:

(1) symmetric pushing force at ridge of 10 MPa across a 100 km thick plate

(2) pulling force at trenches of magnitude 10 MPa

(3) resistive force at continental collision zone, of magnitude 10 MPa

(4) a drag stress proportional to the plate velocity

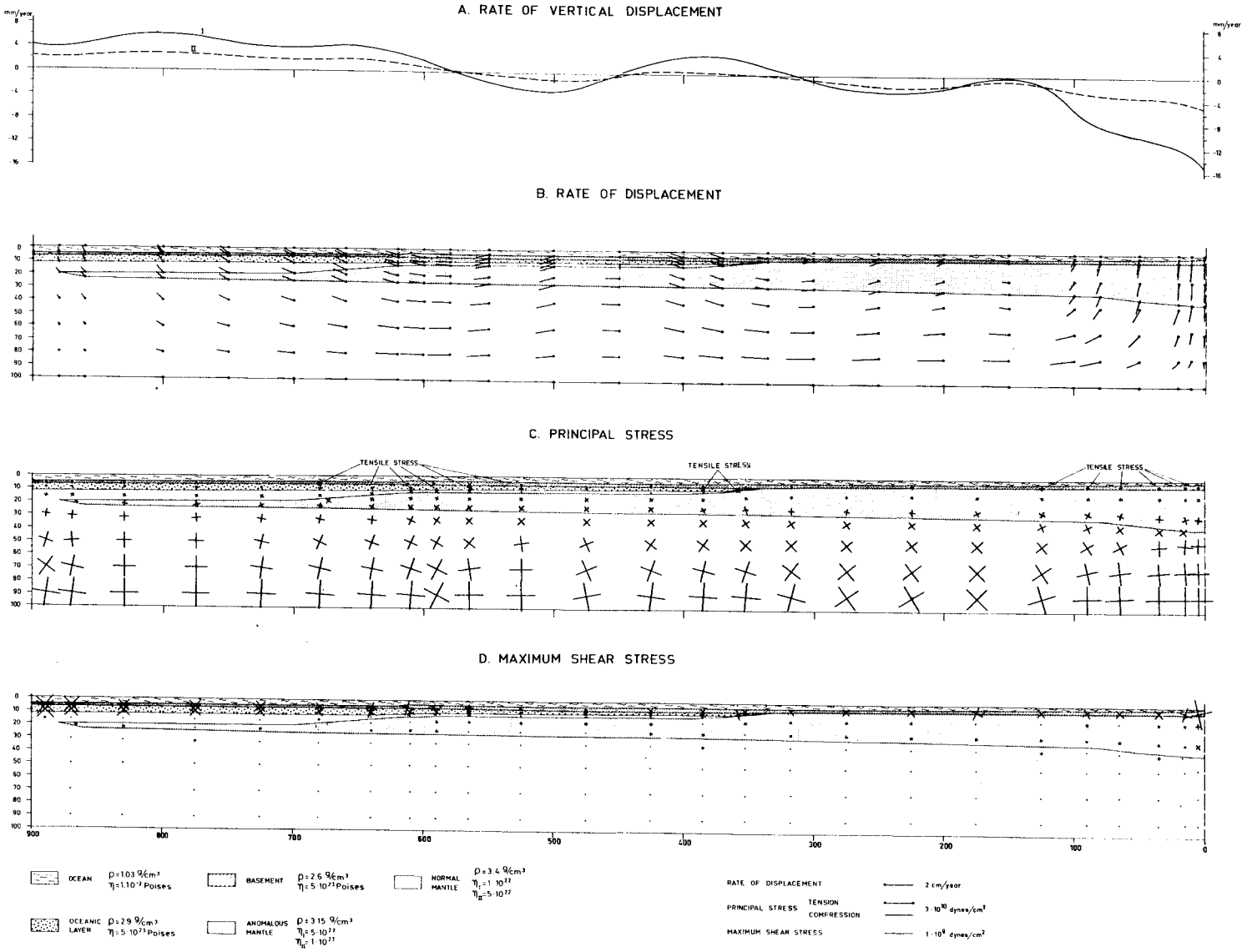


Fig. 2.8 Crustal model of the western flank of the Mid Atlantic Ridge. For explanation, see text. After Stephansson and Berner (1971).

The magnitude and orientation of principal horizontal deviatoric stress for the model of plate driving forces is reproduced in Figure 2.9. Notice the general stress distribution in the Eurasian plate from the Mid Atlantic Ridge to the Pacific french and the direction of the horizontal stress in the cratons on each side of the ridge, cf. Figures 2.3, 2.6 and 2.9.

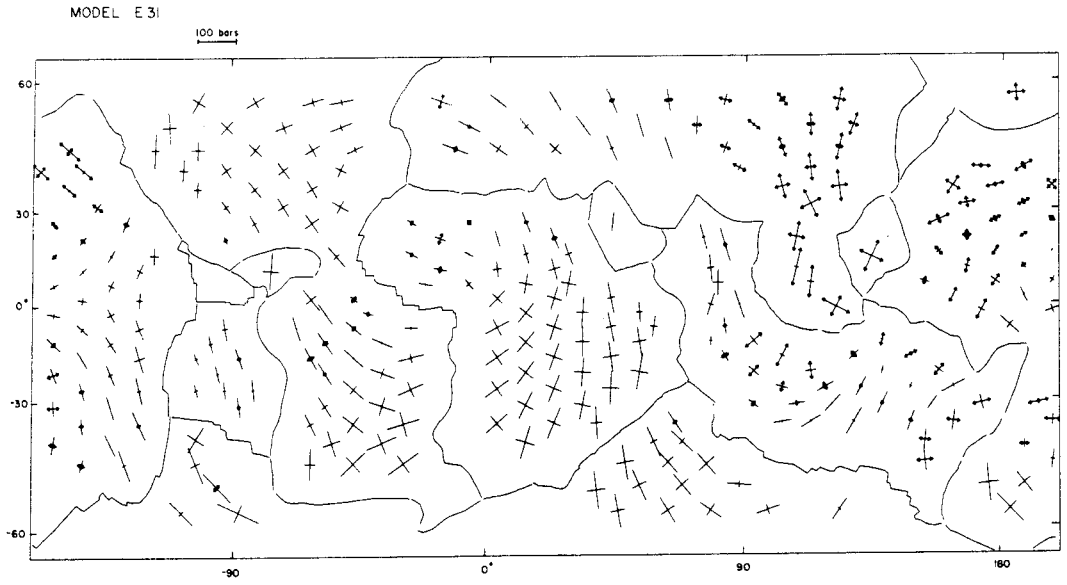


Fig. 2.9 Principal horizontal deviatoric stresses in the lithosphere for a model of plate driving forces (see text). Principal stress axes without arrows and with arrows pointing outwards denote deviatoric compression and tension, respectively. Relative magnitudes of principal stresses is indicated by the length of the stress axes. After Solomon et al. (1980).

The modelling by Solomon et al. (1980) and the single-plate elastic finite element modelling of the North American plate by Reding (1984) give confidence in allowing a rigid push of the order of a few tens of megapascals at the boundary of the plates and demonstrate that regional uniformity of tectonic stresses is possible. However, it does not give us any hint on the stress changes with depth.

The fact that the viscosity is effectively infinite in the brittle and elastic upper lithosphere, but that the viscosity is finite and de-

creases with depth, means that applied push forces at the ridges will be concentrated in the upper lithosphere as a result of creep and stress decay in the lower lithosphere. This effect of stress amplification in the upper lithosphere of a shield area was studied by Bott and Kusznir (1984). After initial application of a uniform compressive stress of 10 MPa across a 150 km thick lithosphere, and assuming power law creep, they obtained a stress distribution as shown in Figure 2.10. Stress relaxation by creep in the lower lithosphere results in progressive amplification of the upper lithospheric stress and gives rise to stress differences of the order of 20-25 MPa during over a time span of 1-100 My.

The most recent and also very attractive model of upper crustal stresses and vertical stress migration of a shield type lithosphere has been conducted by Hasegawa et al. (1985).

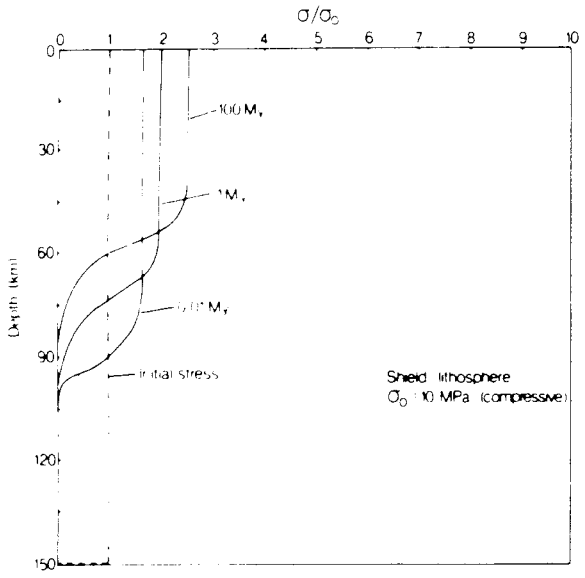


Fig. 2.10 Horizontal stresses within "Shield" types of lithosphere, shown as a function of time after initial application of a uniform compressive stress of 10 MPa across a 150 km thick lithosphere, assuming power law creep. The horizontal stress is normalized with respect to the initial uniform stress shown as a dashed line. Stress relaxation by creep in the lower lithosphere results in progressive amplification of the upper lithosphere stress. After Bott and Kusznir (1984).

Based on existing knowledge of the rheology of the crust and the upper mantle they studied a three-layered model of the Canadian Shield. Since the overall geological evolution is very similar for Canada and Fennoscandia, the model is most applicable for the crustal rock mechanics of this study. Figure 2.11 A shows one of the three-layered plane strain models that have been selected for finite element calculations. The boundary conditions are kept as simple as possible with a free surface and fixed boundaries at the shield and bottom of the upper mantle respectively. A spreading ridge stress of $\sigma_o$ = 10 MPa is applied to the continental lithosphere; the vertical extent of this applied stress corresponds to the thichness of the oceanic lithosphere. The effect of gravity is omitted in the calculations.

The linear rheological model selected is kept as simple as possible. This is shown in Figure 2.11 B and its constitutive equation is

$$\sigma + p_1\dot{\sigma} = q_o\varepsilon + q_1\dot{\varepsilon} \qquad (2.1)$$

where $\sigma$ is the stress, $\varepsilon$ the strain and the overdots denote time differentiation.

$$p_1 = \frac{\eta}{E_1 + E_2}$$

$$q_o = \frac{E_1 E_2}{E_1 + E_2}$$

$$q_1 = \frac{E_1 \eta}{E_1 + E_2}$$

where $\eta$ is viscosity and $E_1$ and $C_2$ are Young's moduli. The values of the relevent parameters for the crust and upper mantle are shown in Figure 2.11 C. The elastic property of the upper crust (layer I) is simulated by assigning to the rheological model an arbitrarly high viscosity value for the crust. For a detailed discussion of the choice of parameters the reader is referred to the original work by Hasegawa et al. (op. cit.).

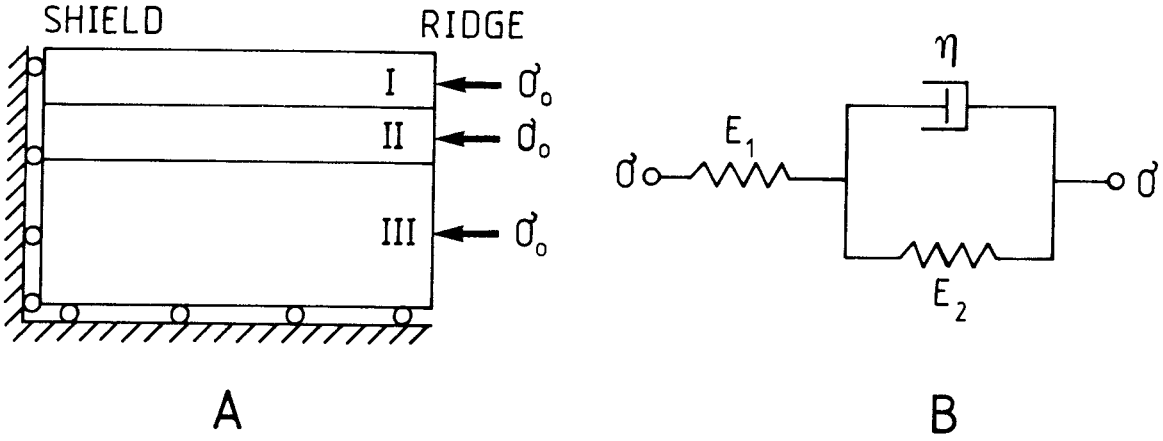


| Layer | Thickness H (km) | Young's modulus $E_1 \cdot 10^{11}$ (Pa) | Young's modulus $E_2 \cdot 10^{8}$ (Pa) | Poisson's ratio $\nu$ | Viscosity $\eta$ (PaS) |
|---|---|---|---|---|---|
| I | 20 | 1.053 | 1.0 | 0.219 | $10^{60}$ |
| II | 20 | 1.284 | 1.0 | 0.197 | $10^{26}$ |
| III | 60 | 1.802 | 1.0 | 0.263 | $10^{23}$ |

C

Fig. 2.11 Linear viscoelastic modelling of the lithosphere. A, finite element model of: I, upper crust, II, lower crust, and III, upper mantle subjected to initial horizontal plate tectonic stress $\sigma_o$; B, viscoelastic model; and C, parameters for three-layered crust-upper mantle model of Canadian Shield. Redrawn from Hasegawa et al. (1985).

Figure 2.12 illustrates the temporal and spatial variation of deviatoric horizontal stress in the three-layered model from time t = 0 to t =$10^8$ years. After t = $10^5$ years the stress in the upper mantle has relaxed. Because of mechanical coupling of the layers, the relaxed stress in the upper mantle is now shouldered by the crust and at t = $10^8$ years induced stress in the lower crust "migrates" to the

upper crust. Thus, the model illustrates the tectonic process whereby the maximum horizontal stress migrates upward resulting in a stress amplification of 40-50 MPa in the upper crust over a time span of about $2 \cdot 10^8$ years starting from the most recent opening of the Atlantic ocean. The temporal variation of deviatoric horizontal stress and strain in the middle of the three layers is reproduced in Figure 2.13. The stress and strain field near the center of the model gives the situation at the central part of the Canadian Shield. Notice the small differences between the strain in the middle of the upper crust near the boundary, and centre of the model.

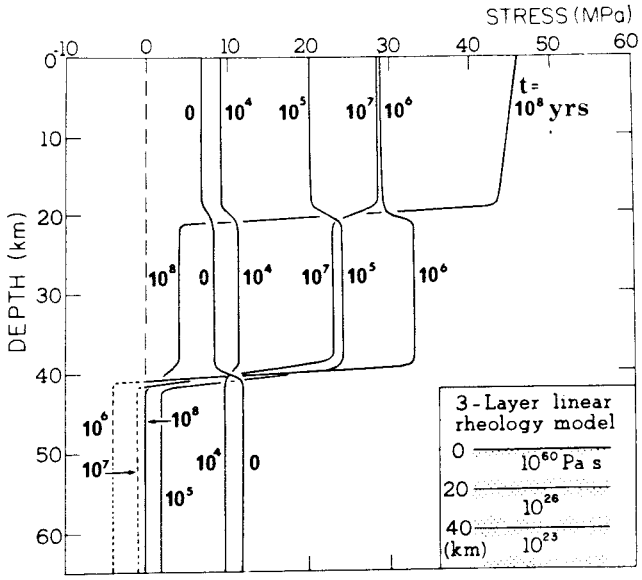


Fig. 2.12 Temporal pattern of horizontal deviatoric stress component for model where 10 MPa horizontal stress is applied to boundary on right to depth of 100 km. Plane strain case shown for three-layered viscoelastic crust-upper mantle model; 0-20 km is upper crust, 20-40 km is lower crust, and 40-100 km is upper mantle. Short dashed-line segments below 40 km represent overshoot at $t = 10^6$ and $10^7$ years, which is a mathematical artifact (i.e, need not occur in reality). After Hasegawa et al. (1985).

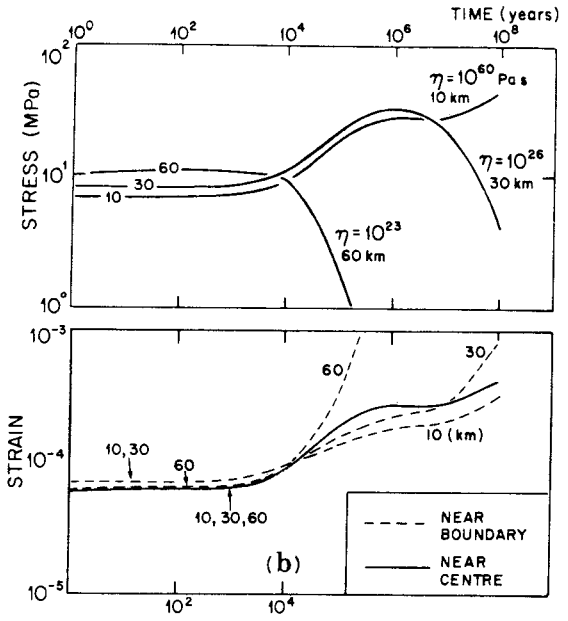


Fig. 2.13 Temporal variation in horizontal stress and strain in middle of upper crust (10 km depth), in middle of lower crust (30 km), and in upper mantle at 60 km depth. Solid curves correspond to central part of Canadian Shield and dashed curves to region closer to spreading center (Mid Atlantic Ridge). After Hasegawa et al. (1985).

Based on the results from the finite element modelling of the elastic-viscoelastic relaxation and contributions from other stress generation mechanisms, Hasegawa et al. (1985) constructed a composite stress diagram for upper (0-20 km) and lower (20-40 km) crust in eastern Canada, Figure 2.14. As stated earlier, a stress situation in eastern Canada is most likely to be applicable also to Fennoscandia. The vertical stress is taken to be equal to overburden stress, $\sigma_V = z \cdot \varrho \cdot g$, and the horizontal differential stresses are measured from this datum. The combined contribution from spreading ridge stress (1) and viscoelastic relaxation (2) is uncertain to within a factor of 3. Residual stress (3) due to incomplete post-glacial rebound is of the order of a few megapascals, for an estimated remaining uplift of 150 m. The contribution from the non-renewable membrane stress (4) is of the order of 10 MPa for a viscoelastic membrane. A deviatoric

stress (5) that increases linearly with depth and is observed in many regions is supposed to be caused by basal drag. Finally, the composite stress field (6) indicates a deviatoric stress that varies from a few tens of megapascals at 5 km to about 100 MPa at a depth of 20 km, i.e. at the base of the upper crust. Below the upper and lower crust interface the horizontal differential stress is governed solely by the spreading ridge stress of 10-30 MPa.

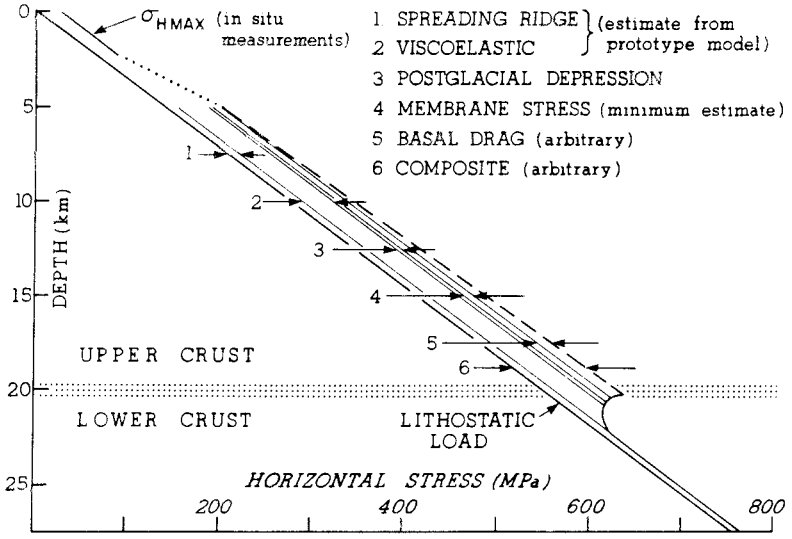


Fig. 2.14 Composite stress diagram for upper (0-20 km) and lower (20-40 km) crust in eastern Canada. Vertical stress is taken to be equal to overburden stress and deviatoric stress levels (represented by separation between arrow pairs) are measured from this datum. Differential stress for 1 and 2 correspond to those of prototype model (for time $t = 10^8$ years after application of 10 MPa spreading ridge stress). Residual stress from postglacial depression is shown in 3. Contribution form viscoelastic membrane stress is shown in 4. Basal drag contribution 5 is shown at an arbitrary level and is intended to illustrate the feature of increasing differential stress with increasing depth. Composite level 6 is arbitrary but tends towards a minimum estimate of deviatoric stress in lower crust. After Hasegawa et al. (1985).

A composite stress diagram for the upper and lower crust in Fennoscandia has been constructed, Figure 2.15. The general state of stress versus depth for $\sigma_{HMAX}$, $\sigma_{HMIN}$ and $\sigma_V$ is in accordance with the measured stresses in the Fennoscandian Shield, cf. Figure 2.1. Earthquake fault plane solutions by Slunga et al. (1984) provide additional information. Many earthquakes are associated with a dominant strike-slip component that would imply that $\sigma_{HMIN}$ is close to $\sigma_V$ and in some areas less than $\sigma_V$. This is the major reason for drawing $\sigma_{HMIN}$ close to $\sigma_V$ in the composite stress diagram. For Fennoscandia the following stress variations are suggested

Upper crust, z = 0-20 km

$$\sigma_{HMAX} = 5 + 32 \cdot z$$

$$\sigma_{HMIN} = 2 + 28 \cdot z$$

$$\sigma_V = 27 \cdot z$$

Lower crust, z = 20-40 km

$$\sigma_{HMAX} = 560 + 30\ (z - 20)$$

$$\sigma_{HMIN} = 540 + 30\ (z - 20)$$

$$\sigma_V = 540 + 30\ (z - 20)$$

where the depth, z, is in kilometres and stresses are expressed in megapascals.

If the effect of gravity is omitted, it is suggested that the variation of differential horizontal stresses with depth z are as follows:

Upper crust, z = 0-20 km

$$\sigma_{HMAX} = 5 + 5 \cdot z$$

$$\sigma_{HMIN} = 2 + z$$

Lower crust, z = 20-40 km

$\sigma_{HMAX} = 20$

For two-dimensional plane strain modelling of vertical sections of the earth's crust, only the maximum horizontal deviatoric stress $\sigma_{HMAX}$ must be applied. For the upper mantle, viscoelastic relaxation acts and zero deviatoric stresses are therefore assumed. As stated in the previous section, there is a strong belief that the regional in-situ stress field in the southern and central part of the Fennoscandian Shield has a NW-SE orientation.

Bäckblom (personal communications) has pointed out that it appears that seismicity in the Fennoscandian Shield decreases as we proceed from the Norweigian coast towards the east. This might reflect decreasing stresses from the edge of the Eurasian plate to the east. If this is the case one would also expect to find a similar reduction in the strain away from the Mid Atlantic Ridge. This idea appears to be supported by results from the analysis presented by Hasegawa et al. (1985) cf. Figure 2.13. In their analysis of the strain near the ridge and also near the boundary of the model, i.e. at the intraplate region, they found the strain to be less near the boundary. Hence, based on the strain distribution and hence the strain energy release predicted by the mathematical modelling one would expect the seismicity to decrease away from the ridge, a situation observed in Fennoscandia.

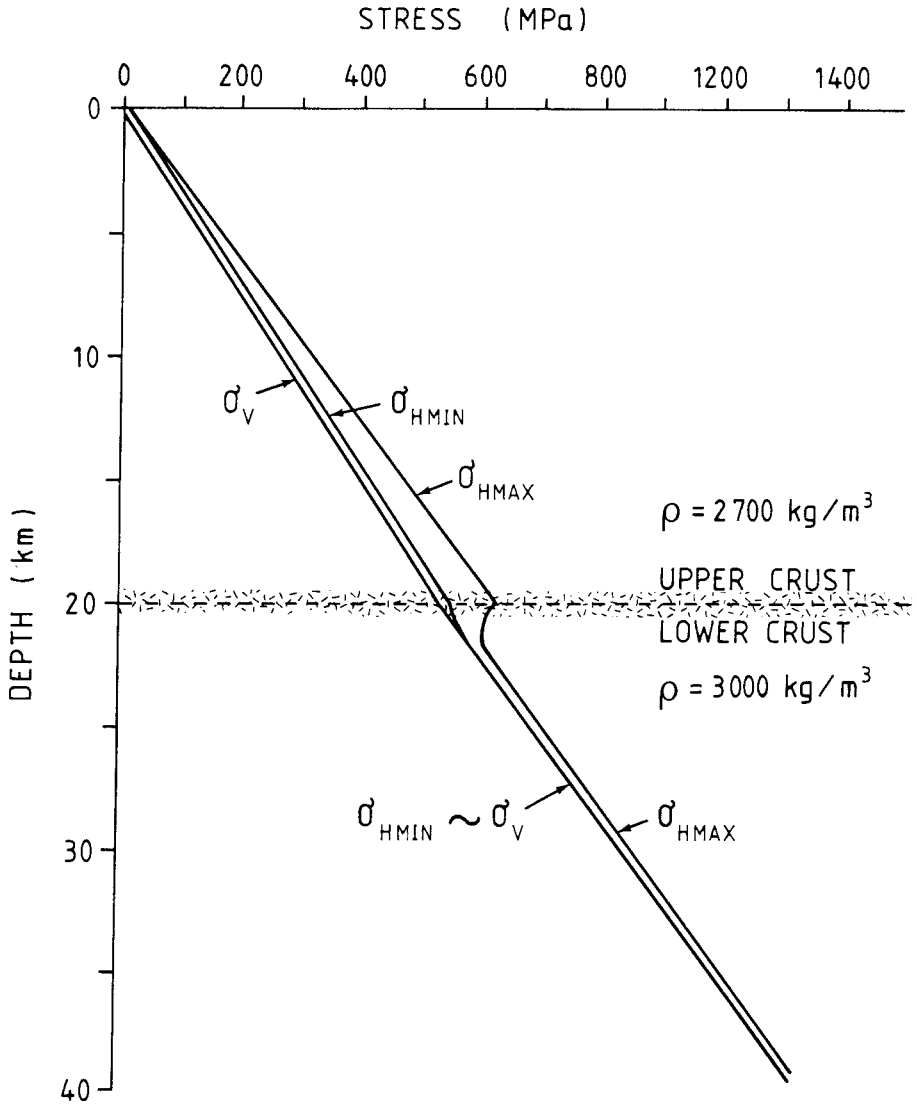


Fig. 2.15 Composite stress diagram for upper and lower crust in Fennoscandia. Stress gradients are in accordance with shallow stress measurements and are most often associated with thrust fault type earthquake fault plane solutions. Absolute stress levels are from the stress diagram of Hasegawa et al. (1985), cf. figure 2.14.

# 3 MODELLING OF FENNOSCANDIAN FAULT STRUCTURES

In a recent report for SKB, Tirén (1986) presents a review of fractures and fracture zones and their structural elements, character and tectonic environment. It forms a comprehensive source of information on the state of art in the structural geology of fractures, faults, fracture zones and shear zones. Fundamental questions which must be raised in modelling large scale faulting and instability in continental shield areas are the following:

- what is the depth of penetration of major fault zones?
- are the deviatoric stresses associated with crustal faulting of the order of 10 MPa or 100 MPa, on average?
- how does shear resistance and strain energy concentration vary with depth?
- how is the faulting developed at the decoupling zone between the upper and lower crust?

To this list of questions, ambiguity will arise from the very sparse information on the brittle and brittle-ductile structures of the Fennoscandian Shield. In this chapter, we will discuss continental fault structures, existing data on fault structures in Fennoscandia, and finally we will suggest a possible fault structure for the modelling of crustal instability.

It is now widely recognized that listric normal faults and thrust faults involving a crystalline basement commonly flatten with depth into décollement zones developed in the middle or lower continental crust (Sibson, 1983 and Jackson and McKenzie, 1983). This makes the alternative models for the downward continuation of major fault zones as suggested by Sibson (op. cit.) most attractive. His alternative models are reproduced to the right in Figure 3.1. For the strik-slip faulting, he suggests two alternative models as the situation is rather more complex. The depth to the decoupling zone within the crust is estimated to be 20 $\pm$ 5 km and will hence coincide with the upper-

lower crustal boundary for the composite stress diagram of the Fenno-scandian Shield, cf. Figure 2.15. The downward continuation of the major fault zones in the continental crust are supported by a conceptual model schematically relating faulting mode, metamorphism, quartz deformation and associated fault rocks, Figure 3.2. From this diagram we notice that the boundary between the discontinuous-frictional-seismogenic upper crust, and the continuous-quasi-plastic-aseismic lower crust is suggested to be at a dept of 12 km and a transition zone reaching down to 15 km. Since the shear resistance and strain energy density diminish at about 20 km this is a realistic boundary between the upper and lower crust in this study.

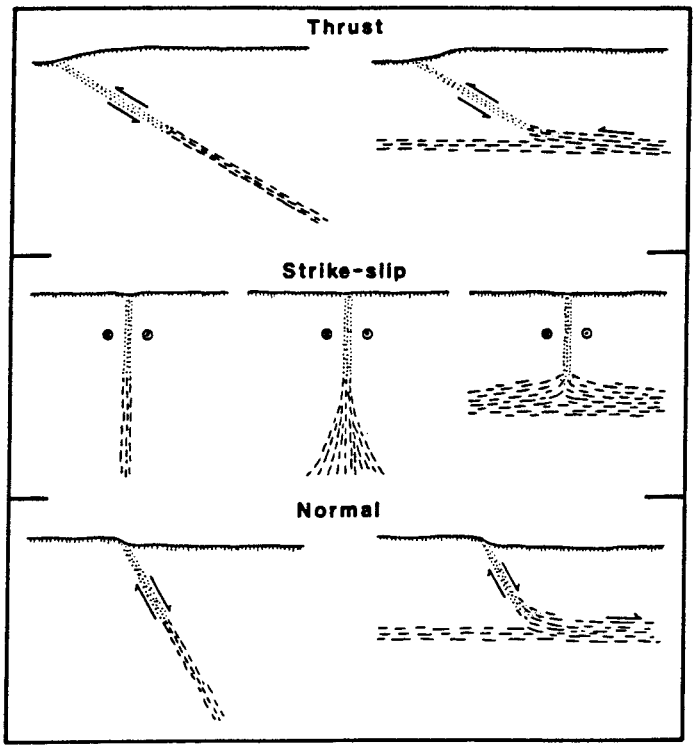


Fig. 3.1 Alternative models for the downward continuation of major fault zones (frictional régime dotted, quasi-plastic shear zones dashed). Suggested models for Fennoscandian faults are shown to the right. After Sibson (1983).

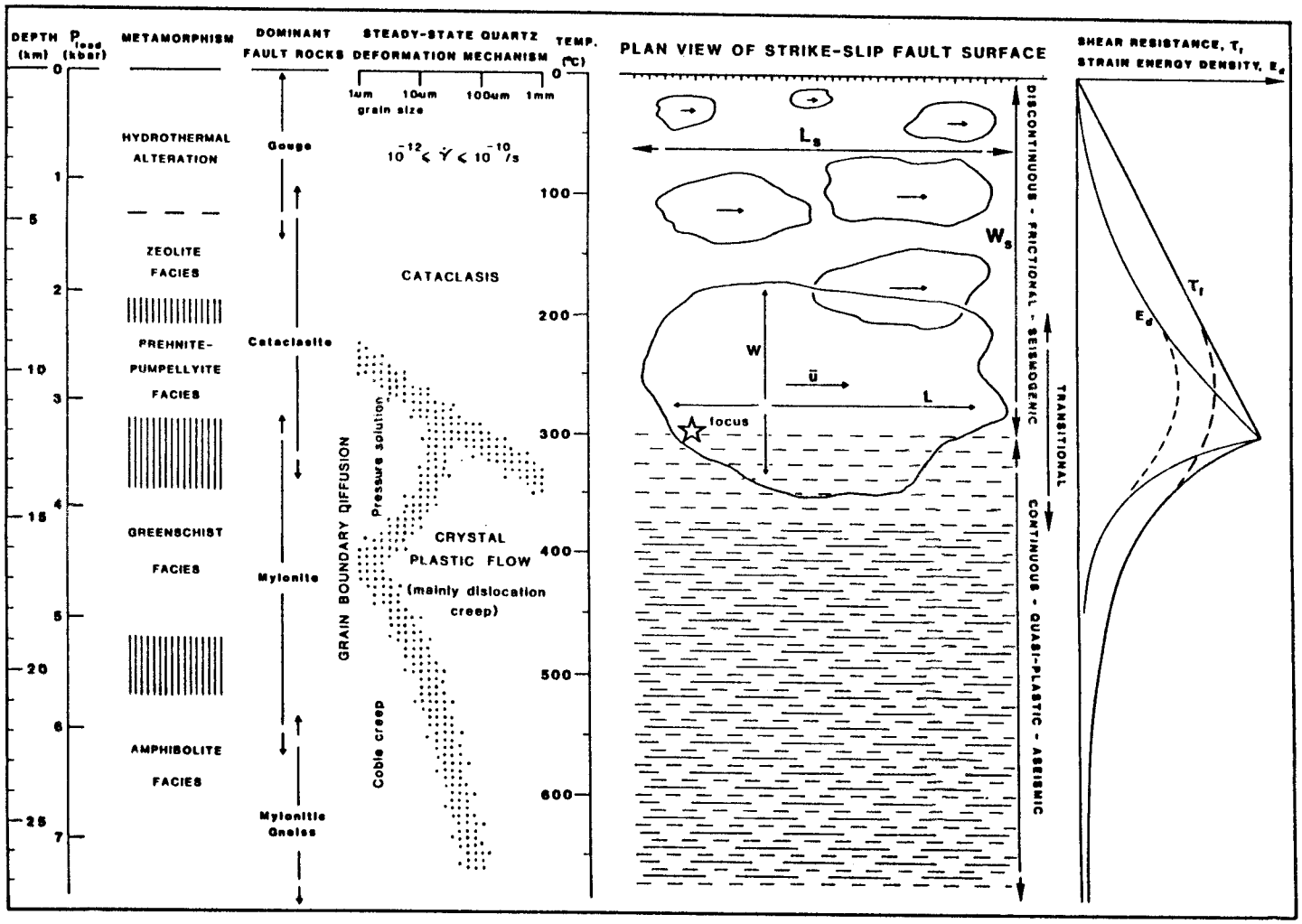


Fig. 3.2 Conceptual model for a major fault zone in the continental crust, schematically relating faulting mode, metamorphic environment, dominant steady-state quartz deformation mechanism and associated fault rocks. Profiles of shear resistance and distortional strain energy density versus depth are in arbitrary units. After Sibson (1983).

The distribution of southern Fennoscandian earthquake foci with depth (Slunga et al. 1984) indicates a confinement of earthquake activity to the upper crust, and this activity is limited to a depth of about 20 km. Hitherto, the evolution of the Fennoscandian Shield has been described mainly from a stratigraphic point of view. Plate tectonic implications, apart from faulting related to neotectonics (Lundqvist and Lagerbäck, 1976, Lagerbäck, 1979, Lagerbäck and Witschard, 1983, Henkel et al. 1983 and Talbot, 1986), and applications have increased in number in recent years. However, the number of studies dealing with faults and shear zones is still limited (Pesonen and Neuvonen, 1981, Eriksson and Henkel, 1983, and Berthelsen and Marker, 1986). A list of published papers and reports on the tectonics of Sweden is presented by Tirén (1986).

In a recent paper, Berthelsen and Marker (1986) presented the tectonic evolution of the Svecokarelian fold belt and presented evidence for large-scale intraplate strike-slip movements along ductile megashears, or strike-slip faults. Associated with the post-collisional stages of the Svecokarelian evolution around 1.9 Ga ago, the formation of a system of large megashears was named as follows:

BB-BB Baltic-Bothnian

R-L Raahe-Ladoga

NK-NK North Karelian

The map of this system is reproduced in Figure 3.3. Although it is still not possible to interrelate the megashears and active subduction zones, the evolution gives some support for a plate tectonic evolution of Early Proterozoic geodynamics of the Baltic Shield. If present-day fracture displacement and seismicity are largely confined to repeated reactivation along the megashears, the latter can be used to define the boundaries of the crustal rock mechanics models of this study. Hence, the Baltic-Bothnian megashear is a strong candidate for the eastern boundary for some of the models. This is further supported by the fact that the BB-BB magashear intersects the area of maximum total glacial uplift and the present maximum of the rate of uplift. The NW-SE striking faults and shears are additional characteristic features

of the structural map of the Baltic-Bothnian region as depicted by Berthelsen and Marker (op. cit.).

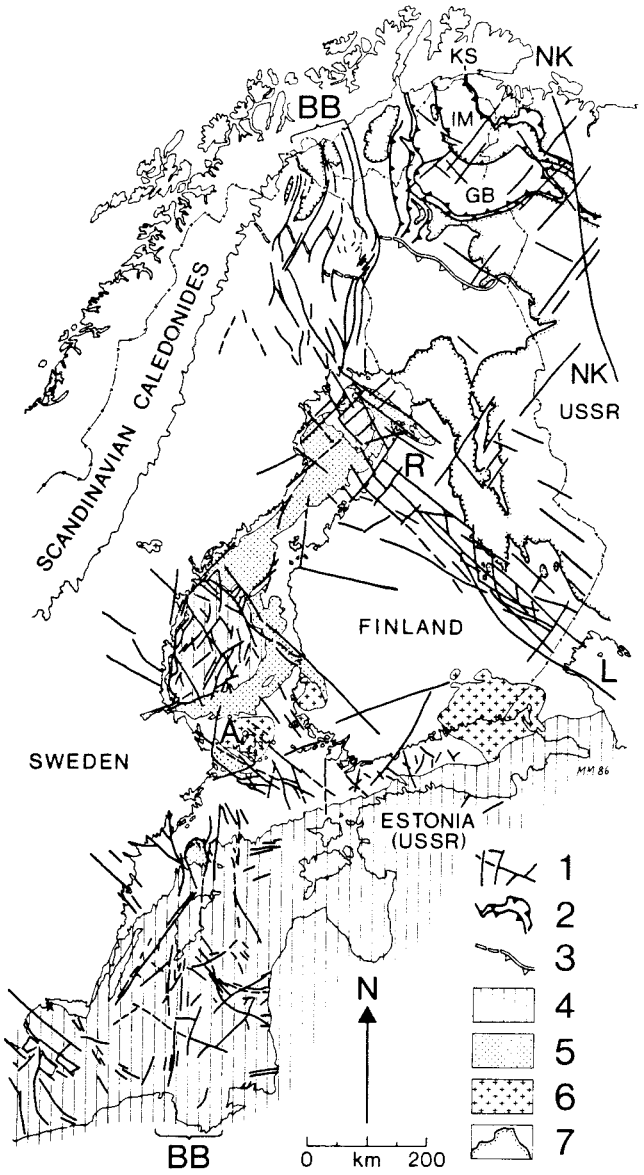


Fig. 3.3 Structural map of the Baltic Bothnian region with offshore geology included to outline the Baltic-Bothnian megashear. 1 = faults and shears, 2 = low-angle thrusts, 3 = the Sirkka line, 4 = Phanerozoic sediments (Vendian included), 5 = Jotnian sediments, 6 = rapakivi granite massifs, 7 = Archaean basement (dotted side). BB-BB - Baltic-Bothnian megashear, R-L - Raahe-Ladoga megashear, NK-NK - North Karelian megashear, KS - Kola suture, IM - Inari microcontinent, GB - Granulite belt, and Å - Åland Archipelago. After Berthelsen and Marker (1986).

A compilation of gravity and magnetic data over Scandinavia, by Eriksson and Henkel, provided the basis for an interpretation of major structural features of the Precambrian bedrock (Eriksson and Henkel, 1983). They distinguished three major sets of lineaments striking N-S, NW-SE, and NE-SW and the traces of two of the transform faults within the North Atlantic ocean basins, i.e. Jan Mayen and Senja fault zone, were extended to the continental crust of Norway and Sweden. Zones of magnetic and sometimes both magnetic and gravity anomalies are distinctly interrupted along NW-SE striking lineaments (Eriksson and Henkel, 1983, Figs. 4 and 5). Several of these lineaments have been interpeted as transform faults by Strömberg (1976), and they form first order lineaments in Central and Northern Scandinavia.

Geophysical investigations, and magnetic mapping in particular, of large-scale regional dislocations in the Lansjärv area of post-glacial faulting in Northern Sweden show two major dislocation trends, NW-SE and N-S (Henkel et al. 1983). From the map of magnetic dislocations, 13 major zones have been interpreted varying in width from 100 m to 1 km and with a mean spacing of about 17 km, Figure 3.4. The dominant strike direction of the major zones is NW-SE over a length of more than 200 km and they are intersected by younger N-S trending zones, showing vertical block movements.

Talbot (1986) made a preliminary structural analysis of the pattern of post-glacial faults in the same area. He suggested that < 1 km thick thrust flakes extruded along the NNE trending fault by oblique transpression along pre-existing steep ESE dipping mega-shears. The post-glacial kinematics inferred from the structures suggest a sudden relief during glacial unloading of plate tectonic forces from horizontal NW or WNW compression accumulated during glacial loading.

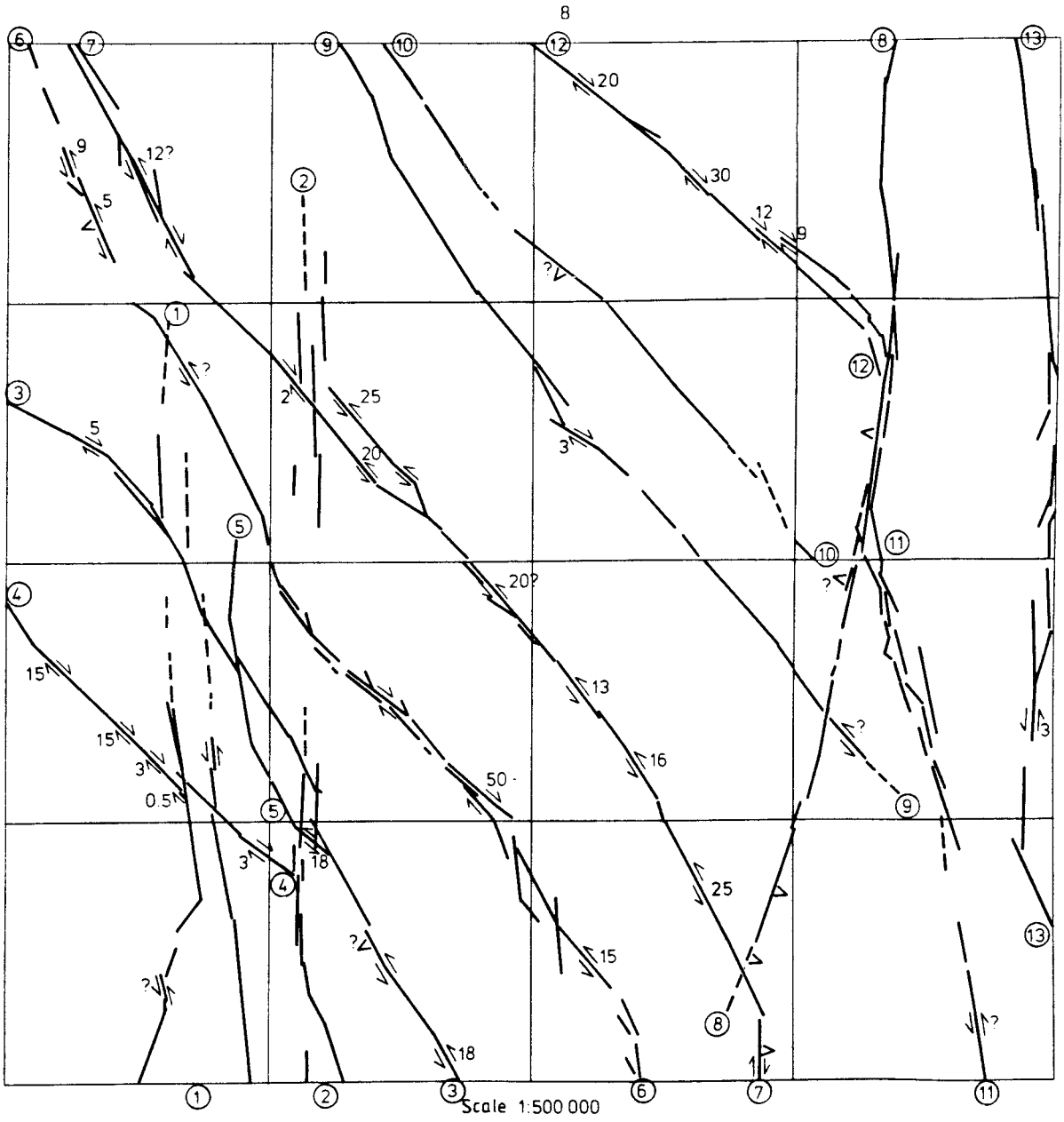


Fig. 3.4 Major dislocations from magnetic mapping of the Lansjärv area, Northern Sweden. The width of the zones varies from about 100 m to 1 km and the maximum extension is more than 200 km. After Henkel et al. (1983).

Figure 3.5 illustrates generic models of vertical and planar sections of Northern Fennoscandia. Boundary conditions are kept as simple as possible and the models are two-dimensional. The vertical section (A) comprises the three-layered model of the lithosphere from the oceanic-continental crustal boundary at the shelf of the North Sea to the centre of uplift in the Bothnian Bay. The Baltic-Bothnian megashear and the centre of uplift are together regarded as a line and a point of symmetry, respectively. Differential horizontal stresses, $\sigma_{HMAX}$, can be applied at the edge of the continental crust. The stress gradients will correspond to the composite stress diagram on crustal stresses and their orientations presented in the previous chapter in the display of faulting in the upper crust (Fig. 3.5 A), steeply dipping N-S striking thrust and strike-slip faults are shown. This situation is based on existing information from the geophysical investigations and geological mapping of the Pärvie and Landsjärv areas (Henkel et al., 1983 and Talbot, 1986). In modelling the crustal stability along the NW-SE profile from the shelf outside Senja in Norway to the northernmost part of the Bothnian Bay at Kalix, additional geological and geophysical mapping is needed. The major structures of the offshore region can possibly be obtained from oil and gas prospecting activities west of Harstad in Northern Norway.

The plan of the NW-SE traverse is shown in Figure 3.5 B. Boundary conditions are the Baltic-Bothnian megashear and applied stresses of $\sigma_{HMAX}$ and $\sigma_{HMIN}$. The fault system for the model must consist of steeply dipping faults and they can be applied as mapped in the field and/or generated by means of existing fracture network modelling techniques, e.g. Mathis (1987). The NW-SE traverse will intersect the major neotectonic structures of the Nordkalott area. Of these, the Lansjärv neotectonic faults are of major interest to this study. In addition the test site for waste disposal at Kamlung will be encountered in the traverse. In modelling the traverse in plan, we are allowed to model an arbitrary horizontal section. At this stage, we suggest modelling at a depth of the mid-upper-crust where differential horizontal stresses are assumed to be $\sigma_{HMAX}$ = 55 MPa and $\sigma_{HMIN}$ = 12 MPa, respectively.

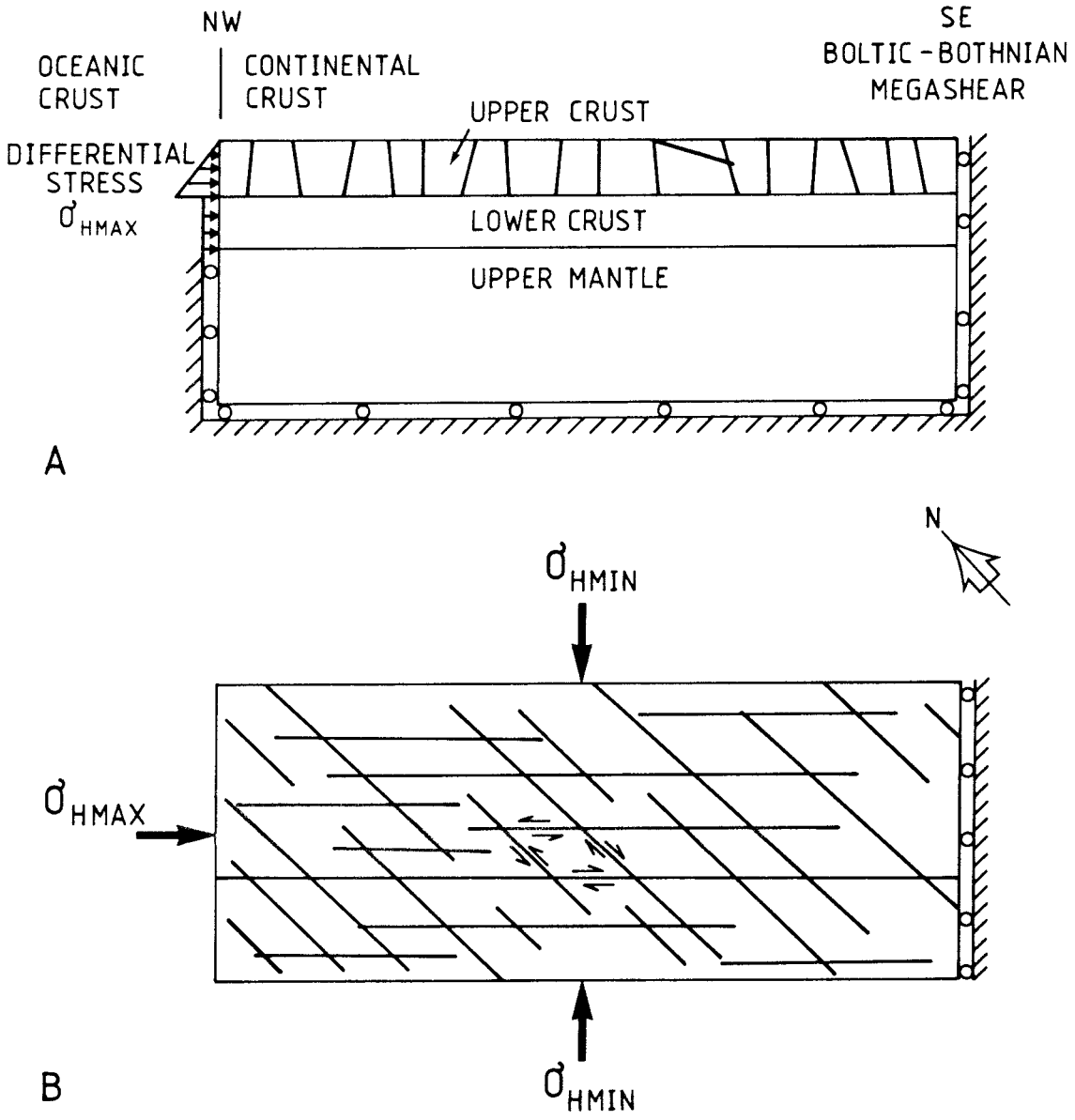


Fig. 3.5 Models of vertical and planar section along a NW-SE travers from oceanic-continental crust boundary outside Senja, Northern Norway, to the northernmost Bothnian Bay.

# 4 GLACIOLOGICAL ASPECTS OF WASTE DISPOSAL IN FENNOSCANDIA

It is known that the location of a nuclear waste vault in the Fenno-scandian bedrock will be affected by large ice sheets in the future. Problems concerning vault integrity under a thick ice sheet have been discussed by Koerner (1984) and Adams (1984), and these are as follows:

(i) erosion of the vault roof by the ice sheet

(ii) increased availability of water and increased water pressure under the ice sheet

(iii) increased stresses on the rock produced by the weight of the overlying ice sheet

(iv) stress relief during deglaciation and cyclic opening and closing of fractures due to repeated glaciations and deglaciations

## 4.1 Erosion under an ice sheet

The general concensus among earth scientists is that ice sheet flow will produce very little erosion relative to the subaerial and fluvial mechanism. In the most recent review of the problem by Koerner (op. cit.) he arrives at an erosion rate of 1.5 m in 0.1 Ma, corresponding to 15 m in 1 Ma. The present conclusion is that glacial erosion does not constitute a threat to a repository situated deeper than a couple of hundred metres. The effects of erosion need not therefore be simulated in the numerical modelling of crustal rock mechanics.

## 4.2 Water pressure under the ice

One of the principal sources of uncertainly in the storage of high-level radioactive waste in the bedrock of Fennoscandia arises from the effects of increased water availablity and water pressures associated with large ice sheets. Koerner (1984) presents evidence that the rock

surface will have a water interface for most of the time when it is covered by an ice sheet. This will result in the development of excess pore-water pressure and the volume of water flow above the repository could be at least 3 to 6 times greater than it is at present. The basal water film at the base of the ice sheet may be only millimetres thick, but the hydrostatic pressure at the bed could be sufficiently high for water to penetrate new or old fractures in the bedrock. It might also be possible that the excess water pressure could cause hydraulic fracturing of the surface bedrock as has been suggested by Pusch (personal communication). An additional effect is the reduction of basal shear stress of the ice sheet by a factor of 2 to 4 according to Koerner (op. cit.)

There is no general agreement on the precise location of the water table within an ice sheet. Vonhof (1984) does not think that the ice surface may be considered equivalent to a zero potential surface. In a discussion of the contribution by Vonhof (op. cit.) Fischer claims that for temperate glaciers, water will move through a glacier, and the concept of a water table in a glacier, coupled with the one in the grounds been proposed. The present knowledge of water tables in continental glaciers is however more uncertain. Fischer also considers that there is a good chance for melting at the bottom of the centre in a continental glacier. Further up, the temperature of the ice would probably quickly drop to below $0^{o}$ C. Based on temperature calculations, Koerner (op. cit.) shows on the contrary that the ice sheet is frozen to its bed in the accumulation zone. However, there is a general concensus that high water pressures can develop in the ablation zone.

In conclusion, in any simulation of the displacement and stress changes under glacial loading, changes of pore water pressure in the bedrock due to changes in the water table of the ice sheet must be considered.

## 4.3 Glacially induced stress changes

An ice sheet produces differential loads over the earth's crust. By

assuming an infinite extension of the ice and linear elastic properties of the crust, the theoretical horizontal stress would increase by an amount $\Delta\sigma_H$ given by

$$\Delta\sigma_H = \frac{\nu}{1 - \nu} \Delta\sigma_V \qquad (4.1)$$

where $\nu$ is the Poisson's ratio and $\Delta\sigma_V$ is the glacial overburden load from the ice sheet. After deglaciation $\Delta\sigma_V$ and hence $\Delta\sigma_H$ vanishes. However, an ice sheet will produce differential loads over the earth's crust, and the ensuing crustal uplift or rebound in Fennoscandia and other glaciated terrains prove that the concept of elastic deformation is not valid.

By studying the nature of the deformation or the distribution of the compensation produced by an ice sheet, the isostatic response of the crust to loading may be assessed. Walcott (1970) studied the isostatic response to ice sheet loading of the crust in Canada in which the lithosphere was treated as an elastic sheet overlying a fluid substratum. By applying the well-known theory of elastic bending of a thin plate in two dimensions, the upward pressure caused by the elastic bending is $D \frac{d^4w}{dx^4}$, where D is the flexural rigidity of the plate and to $ET^3/12(1 - \nu^2)$; E is the Young's modulus, T the plate thickness and $\nu$ the Poisson's ratio. By assuming the profile of the ice sheet is

$$h = h_o (1 - e^{bx}) \qquad (4.2)$$

where, h is the elevation and $h_o$ the elevation as $x \rightarrow -\infty$ and b a constant, the vertical displacement w of the ground surface at each side of the ice edge is given by the following equation:

$$\frac{d^4w}{dx^4} + 4a^4w = \frac{h_o (1 - e^{bx}) \varrho_i g}{D} \qquad x < 0 \qquad (4.3)$$

and

$$\frac{d^4w}{dx^4} + 4a^4w = 0 \qquad x > 0 \qquad (4.4)$$

where

$$4a^4 = \frac{(\varrho_m - \varrho_i)\, g}{D} \qquad (4.5)$$

In eqs. 4.3 - 4.5 above $\varrho_m$ is density of mantle, $\varrho_i$ is density of ice and g is the acceleration of gravity. The calculated surface profile at the edge of a continental ice sheet with radius 450 km and elevation 1.8 km is shown in Figure 4.1. From the solution of the above differential equations, the following three features should be noted:

(i) a forebulge is produced because of the elastic bending. Its amplitude is independent of the flexural parameter D and is given approximately by $h_o/100$. The distance from the ice edge at which the forebulge occurs depends on the flexural rigidity and is given approximately by $1.9 \cdot 1/a$

(ii) at the ice edge, the ground surface is depressed by a distance of $h_o/11.5$. The turning point of the displacement, i.e. $w = 0$, occurs when $ax = 1.89$. This point is of special interest in the modelling of the crustal rock mechanics in Fennoscandia, since this can be used as a point of symmetry for the NW boundary of the models. The displacement of the ground surface beyond the ice sheet is given by

$$w = \frac{h_o\, \varrho_i}{\varrho_m - \varrho_i} \left[ e^{ax} \left( \frac{\sin ax}{2} - \frac{4}{5} \right) + 1 \right] \qquad (4.6)$$

and outside the ice edge,

$$w = \frac{h_o\, \varrho_i}{10\,(\varrho_m - \varrho_i)} \{ e^{-ax} (2 \cos ax - \sin ax) \} \qquad (4.7)$$

It is suggested that the geometry of the lithosphere on each side of the ice edge is given a shape defined by these equations

(iii) the maximum stress difference will occur at the base of the lithosphere and about 200-300 km from the edge of the ice sheet (Walcott, 1970). The magnitude of this difference is approximately 20 MPa per kilometer of elevation of ice sheet.

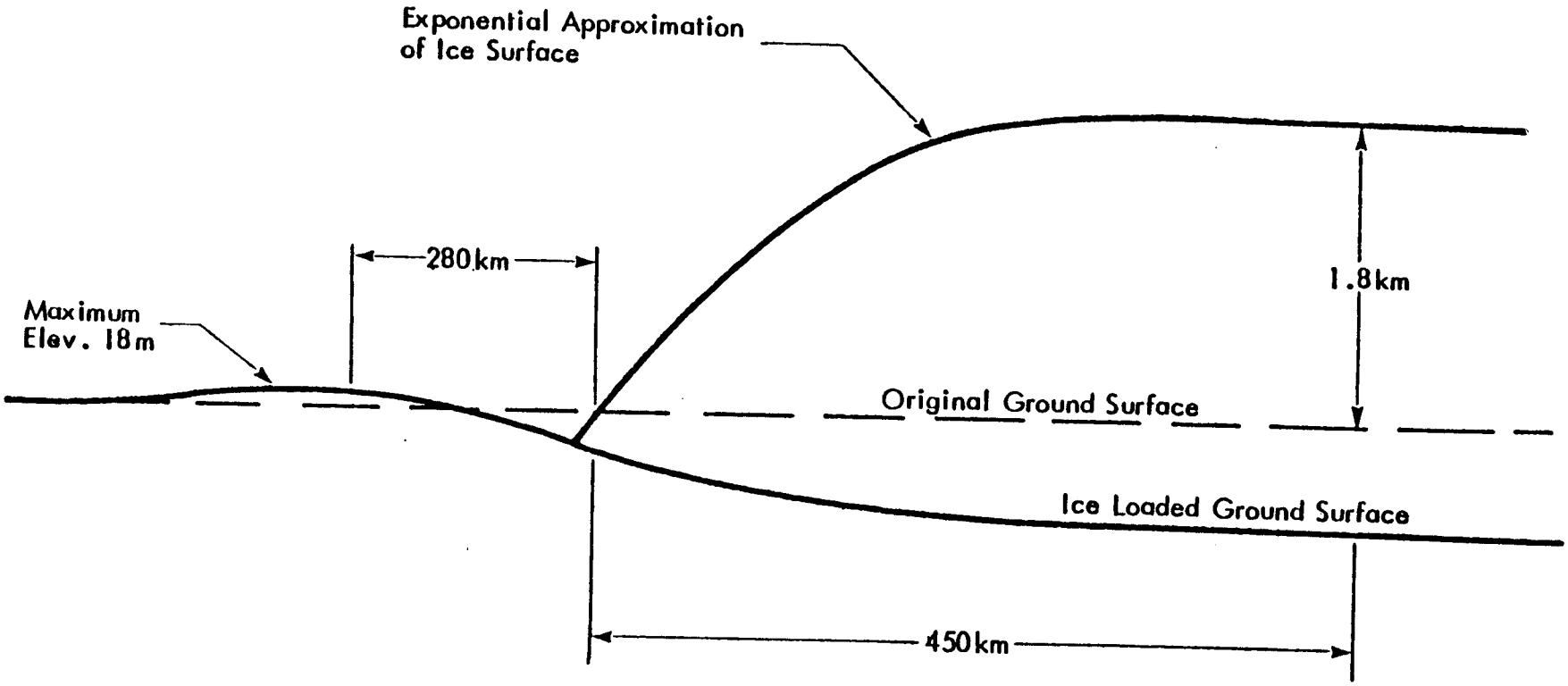


Fig. 4.1 Profile across an ice front. After Walcott (1970).

The maximum horizontal stress at the upper surface of the upper crust is estimated to be 8.5 MPa per kilometer elevation of ice. Hence, for an ice sheet of 2 km thickness, the horizontal stress due to subsidence will be 17 MPa, and compressive at the upper surface of the crust and tensile at lower surface.

## 4.4 Stress concentration at the ice-rock interface

Although much thought has been given to the glacial sliding, bed-water-ice interface problem, a detailed description of a problem formulation at any given time does not appear in the litterature. Weertman (1979) has reviewed the theory of glacial sliding, and the following section is based on his contribution.

Let us consider any arbitrary block of ice that is within a glacier and which is just above the bed, Figure 4.2.

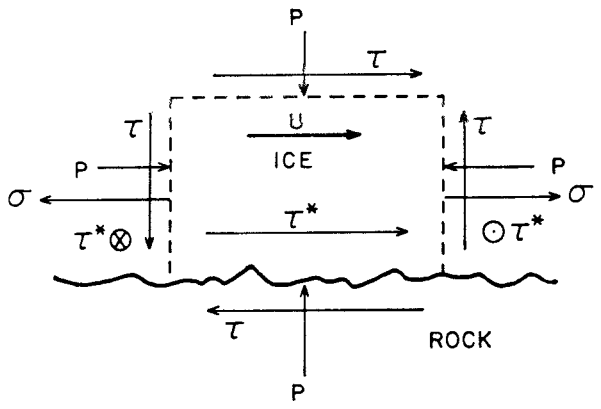


Fig. 4.2 Block of basal ice sliding over a glacier bed. After Weertman (1979).

The following parameters have been considered in glacial sliding theories or have been thought to influence glacial sliding:

1) The average shear stress $\tau$ that acts parallel to the glacier bed (Fig. 4.2). Presumably the direction in which this basal shear stress acts is parallel to the average direction of the velocity U.

2) The average hydrostatic pressure P that acts on the ice block (Fig. 4.2).

3) The deviator stresses, one of which is indicated as the stress $\sigma$ in Figure 4.2, that act normal to ice-block faces. The shear stress $\tau^*$ that is indicated in Figure 4.2, acts on the set of ice block sides that are all perpendicular to the bed. This should also be considered with the tensile or compressive deviator stresses.

4) The temperature of the ice as well as the bed.

5) The morphology of the bed surface.

6) The rheological properties of ice.

7) The rheological properties of the bed material.

8) The quantity of water transported per unit time down the glacier within the bed-water-ice interface.

9) The quantity of water ber unit time either reaching the bed-water-ice interface through a permeable bed or escaping from this interface through a permeable bed.

10) The dissolved impurity content of the water at the bed-water-ice interface and the dissolved impurity content of the ice.

11) Rock debris and silt content within the ice.

12) The quantity of geothermal heat transported to the glacier bed.

13) The quantity of water reaching the bottom surface of the glacier from the top surface of the glacier, either through moulins or crevasses that penetrate a glacier or down from the edge of a glacier.

According to Weertman (op. cit.), the bed-water-ice glacier sliding problem is simply the determination of the velocity U of this block of ice shown in Figure 4.2. If we assume a perfectly smooth interface, where the velocity is determined by the water layer in shear, the shear stress is equal to

$$\tau = \eta\, U/d \qquad (4.8)$$

Here, $\eta$ is the viscosity of water $\approx$ 0.0018 Pas and d is the water layer thickness of $\approx$ 1 nm. The average shear stress is found to be of the order of 6 Pa for $U \approx 100\ ms^{-1}$. The average shear stress at the base of a glacier is of the order of 0.1 MPa and many orders of magnitude larger than the generated shear stress in a water layer. If the interface is below the freezing point the tangential stress might reach a value of about 2 MPa so it may to be concluded that a glacier whose bed temperature is below the melting point of ice should not slide.

Weertman was the first to consider a rough interface in glacial sliding theory. For sliding to occur over a protuberance bed model consisting of cubic blocks with side length L and average separation $L^1$, tensile and compressive stresses will exist near each obstacle of the order of $\tau / R^2$ where $R = L/L^1$ is a measure of the roughness of the bed. $\tau$ is the average basal shear stress, of magnitude 0.1 MPa. Hence, obstacles of a height of 20 m with an average distance of 200 m gives R = 10 and $R^2$ = 100 and the tensile and compressive stresses will be of the order of 10 MPa.

The stress concentrations around each obstacle will cause the ice to flow by creep around them, and at a distance of about one obstacle length the stress concentration must die out. Because the normal stress on the up-stream side and the down-stream side differ by an amount equal to $\tau / R^2$, the melting temperature of ice is different.

The temperature gradient causes the ice to melt on the up-stream side and water to be refrozen on the down-stream side. This process is named regelation. The total sliding velocity of an ice sheet over an obstacle is therefore the sum of the velocities from the creep flow and the velocity produced by the regelation mechanism.

Nye analyzed the relation between surface and bed topography of an ice sheet flowing across a small ridge (Paterson, 1972). This problem is relevant to neotectonic faulting in Northern Sweden. If we assume that the flow is constant across the ridge and the change in shear stress produced by the ridge is denoted $\tau_1$, then

$$\tau_1/\tau_b \approx 0.5\ r/h_o \qquad (4.9)$$

where $\tau_b$ is the basal shear stress, r the height of the ridge and $h_o$ is the thickness of the ice sheet. Hence, a ridge with a height of 20 m covered by 2000 m of ice should change the basal shear stress by only 0.5 per cent. Since the calculated basal shear stress is about 0.1 MPa in many parts of polar ice sheets, the change in shear stress caused by the ridge can be neglected.

From the above analyses we may conclude that the problem of glacier slid ing and bed-water-ice interface stresses remains unsolved. For the purpose of our modelling, we assume the following values:

average basal shear stress $\tau_b$ = 0.1 MPa

maximum obstacle compressive/tensile stress $\tau_o$ = 10 MPa

In contrast with the interior of a glacially loaded area, a rock mass at the edge of an ice sheet would experience significant non-uniform loading and high stress gradients (Adams, 1984). The simple calculations presented in this section show that it is unlikely that the stresses would cause major disturbances to the rock mass. For a greater impact, Adams (op. cit.) suggests that either the ice front must have been steeper, or calving of icebergs at the front have generated large shear stresses. Talbot (1986), in his mapping of the neotectonic faults in Northern Sweden suggests that the morphology in the vicinity of the faults can only be explained by large magnitude earthquake ac-

tivity. At the present stage, the final explanation of the neotectonic structure must be left open. Hopefully modelling of glacial sliding and stress concentrations from obstacles will broaden our views and increase knowledge of possible mechanisms.

## 4.5 Modelling of glaciation and land uplift

Fennoscandia is one of the best known and studied postglacial land uplift areas. The present uplift rate has its maximum value, of about 1 m per 100 years, at the centre of the glaciation which is located in the northern part of the Gulf of Bothnia. The absolute land uplift $V_a$ is obtained from the equation

$$V_a = V_o + V_e + V_g \qquad (4.10)$$

where $V_o$ is the observed land uplift rate from tide-gauge and precise levelling observations and $V_e$ is the eustatic rate of rise of the sea level. $V_g$ is the uplift rate of the geoid with respect to the centre of gravity of the earth arising from subcrustal flow of viscous mantle material. The observed land uplift in Northern Europe has been compiled by Ekmann (1977), Figure 4.3. The eustatic rise of mean sea level is considered to be $V_e \approx 1$ mm/a. Uplift of the geoid at the centre of the Fennoscandian land uplift has been calculated by various authors and a recent compilation by Kukkari (1986) gives $V_g$ = 0.7-1.2 mm/a. Based on this data, the additional land uplift has been estimated to be 80 and 140 m and the relaxation time from 7000 to 12000 years.

Mörner (1979) attempted to show that the uplift arises from two causes; an exponential uplift from glacial ice melt (now completed), and also a tectonic uplift (continuing) which is unrelated to the removal of the ice load. However, the present contours of uplift based upon tide-gauge records correspond well with contours of total isostatic uplift and with the distribution of glacial ice. According to Emery and Aubrey (1985) this favours a single, rather than two different causes for uplift.

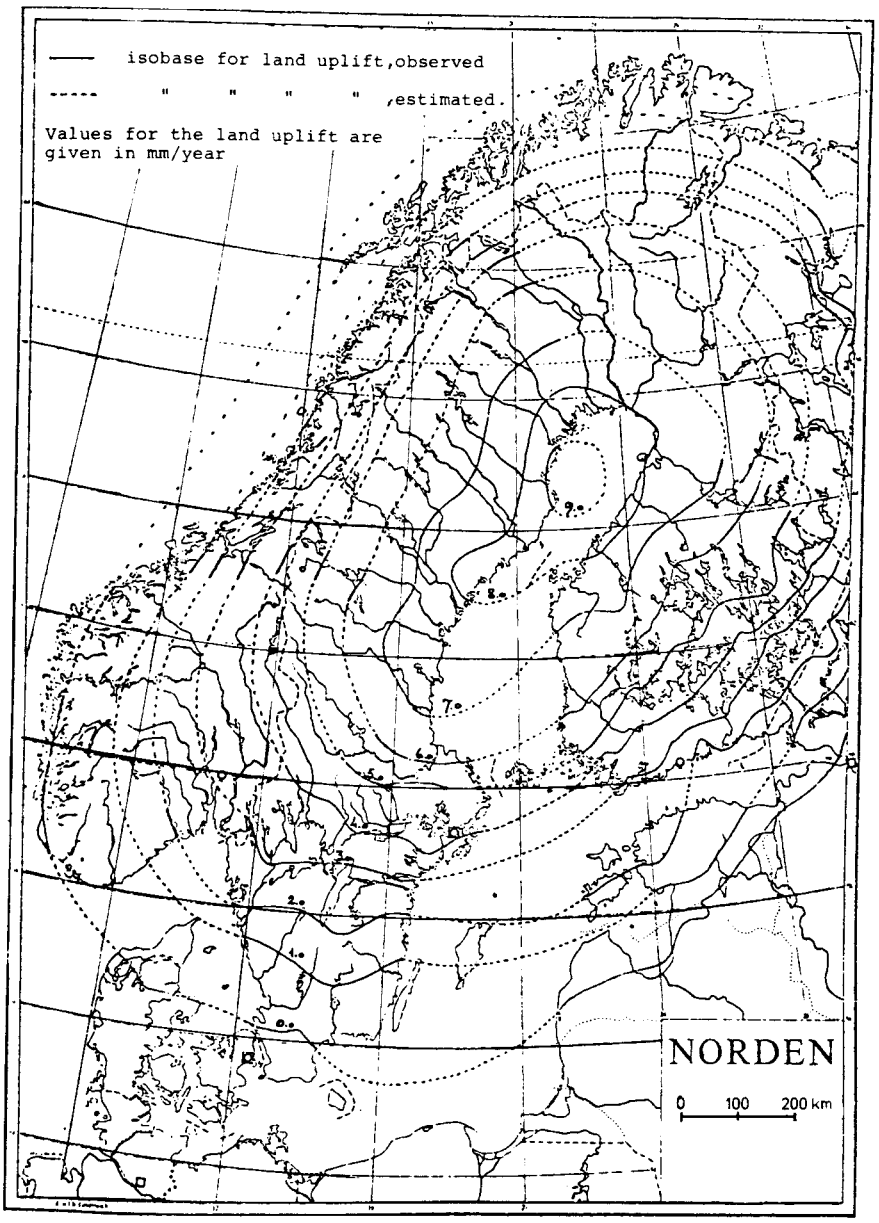


Fig. 4.3 Observed land uplift rate in mm/yr. Compiled by Ekmann, 1977. See Ekmann (1985).

The Weichselian glacial ice began about 75.000 years B.C. and increased to a maximum at about 20.000 years B.C. The maximum ice extension of the Weichselian ice and the ice border at Younger Dryas (10.000-11.000 B.C. and Pre-Boreal (9.000 B.C.) is reproduced after Bakkelid (1986) in Figure 4.4. Notice the similar shape and geographic

extension of the glaciated area and the zero isobase of present uplift rates in Northern Fennoscandia. This further strengthens the idea of using the point of zero vertical displacement slightly west of the ice border as a line of symmetry in the modelling work. The ice divide strikes almost perpendicular to the direction of the suggested traverse of modelling and the ice divide. It is most probable also that the maximum thickness of the ice sheet is located adjacent to the eastern point of the suggested traverse. Hence, the existence of a symmetry line at the NE end of the traverse at Kalix is also supported by the extension of the ice sheet.

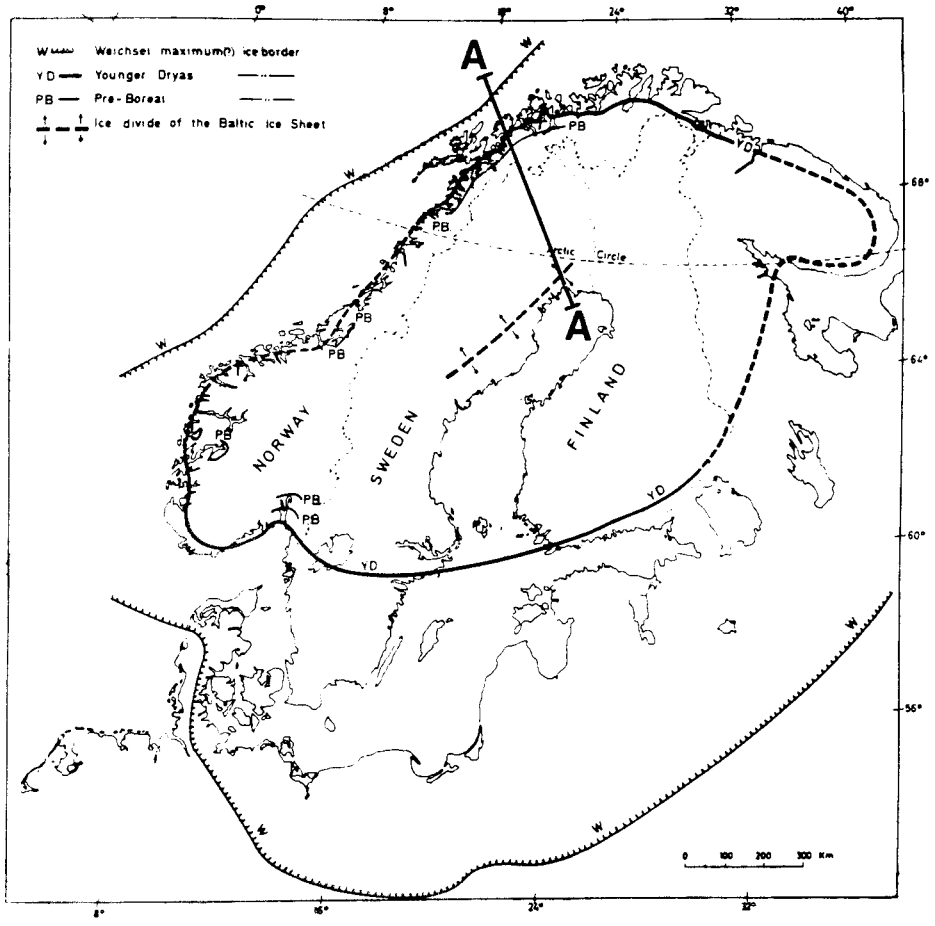


Fig. 4.4 The most important Weichselian ice borders and the ice divide. In the figure is also shown the suggested profile A-A for numerical modelling of crustal rockmechanics. After Bakkelid (1986).

In modelling the influence of glaciation, deglaciation and glacial rebound on crustal rock mechanics and stability, two modelling approaches are suggested. In the first approach, we model the changes of glacio-isostatic deformation as they are assumed. Hence, the surface and bottom of the model is given a shape in accordance with the equations by Walcott (1970), equations (4.6) and (4.7) for each side of the ice front, Figure 4.5 A. The uplift, $\Delta H$, will be varied according to the following scheme:

| | |
|---|---|
| total uplift | $\Delta H$ = 900 m (Kukkari, 1986, Mörner, 1980) |
| present uplift | $\Delta H$ = 760 m (Mörner, 1980) |
| highest shoreline | $\Delta H$ = 295 m |
| remaining uplift | $\Delta H$ = 140 m (Kukkari, 1986) |
| relaxed mantle | $\Delta H$ = 0 m |

We also intend to model an estimated maximum absolute uplift of 760 m as has been suggested by Mörner (1980), although this value has been questioned by several authors, e.g. Emery and Aubrey (1985).

The other modelling approach uses ice as a surface load, Figure 4.5 B. The profile of the ice sheet is assumed to either the equation

$$h = h_o (1 - e^{bx}) \qquad (4.11)$$

or

$$(h/h_o)^2 = 1 - X/L \qquad (4.12)$$

where, h is the elevation, $h_o$ is the elevation at distance L and b is a constant. The edge of the ice sheet agrees with the extension of the Weichselian glacial ice at the continental shelf of Northwestern Norway. The retreat of the ice sheet will be modelled so that the edge will be situated at the neotectonic faults in Northern Sweden for a

remaining ice thickness of about 1 km. It is suggested that the influence of a water table corresponding to a dry frozen glacier and a tempered glacier with a waterhead corresponding to the thickness of the ice is also analyzed.

Global models as presented in Figure 4.5 will make it possible to increase our overall understanding of the change in stresses and deformations. They can also provide the boundary conditions for regional and far-field models as indicated in Figure 4.6. In the regional models, the neotectonic faulting can be studied in more detail by introduction of loading from an ice sheet front, basal shear stress at the rock-ice interface and additional stresses and deformations due to various obstacles at the ground surface underneath an advancing and retreating ice front.

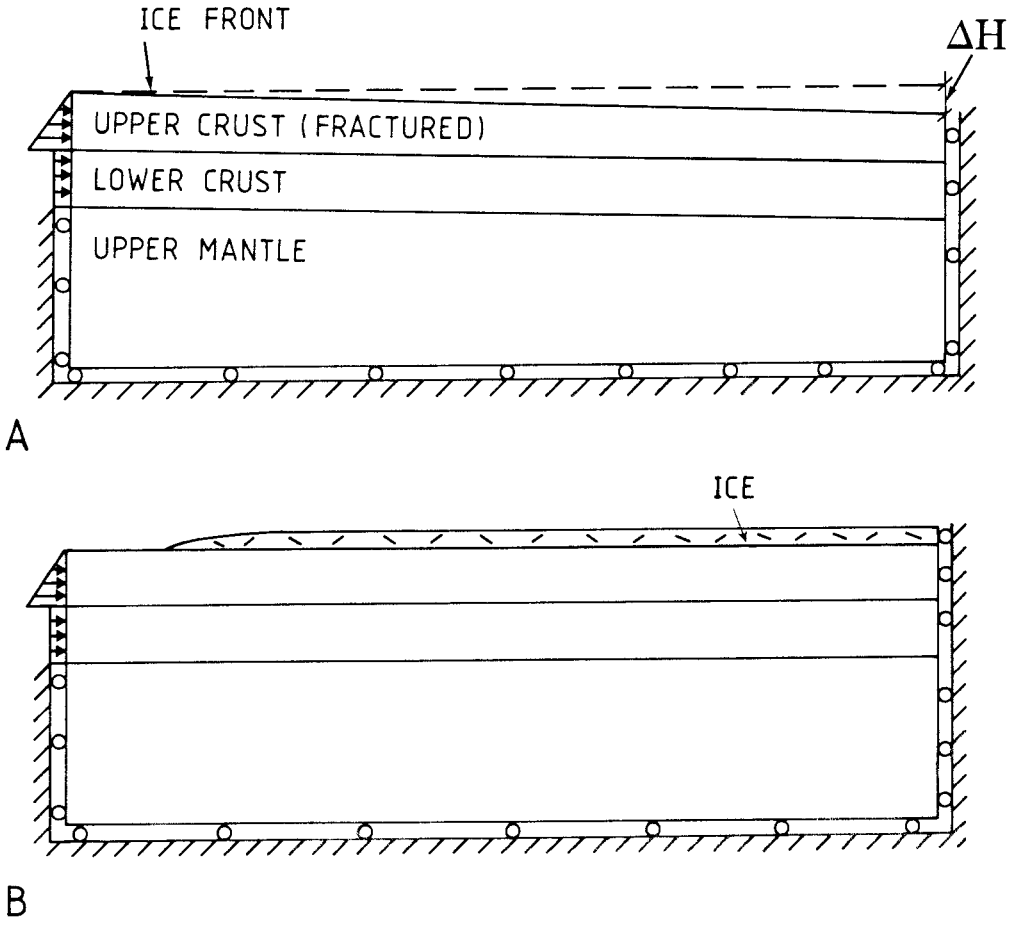


Fig. 4.5 Suggested modelling of glaciation, deglaciation and glacial rebound for a NW-SE traverse in Northern Fennoscandia.
A, Simulation of glacial rebound at the centre of uplift, ΔH
B, Simulation of ice load from a Weichselian glacial ice.

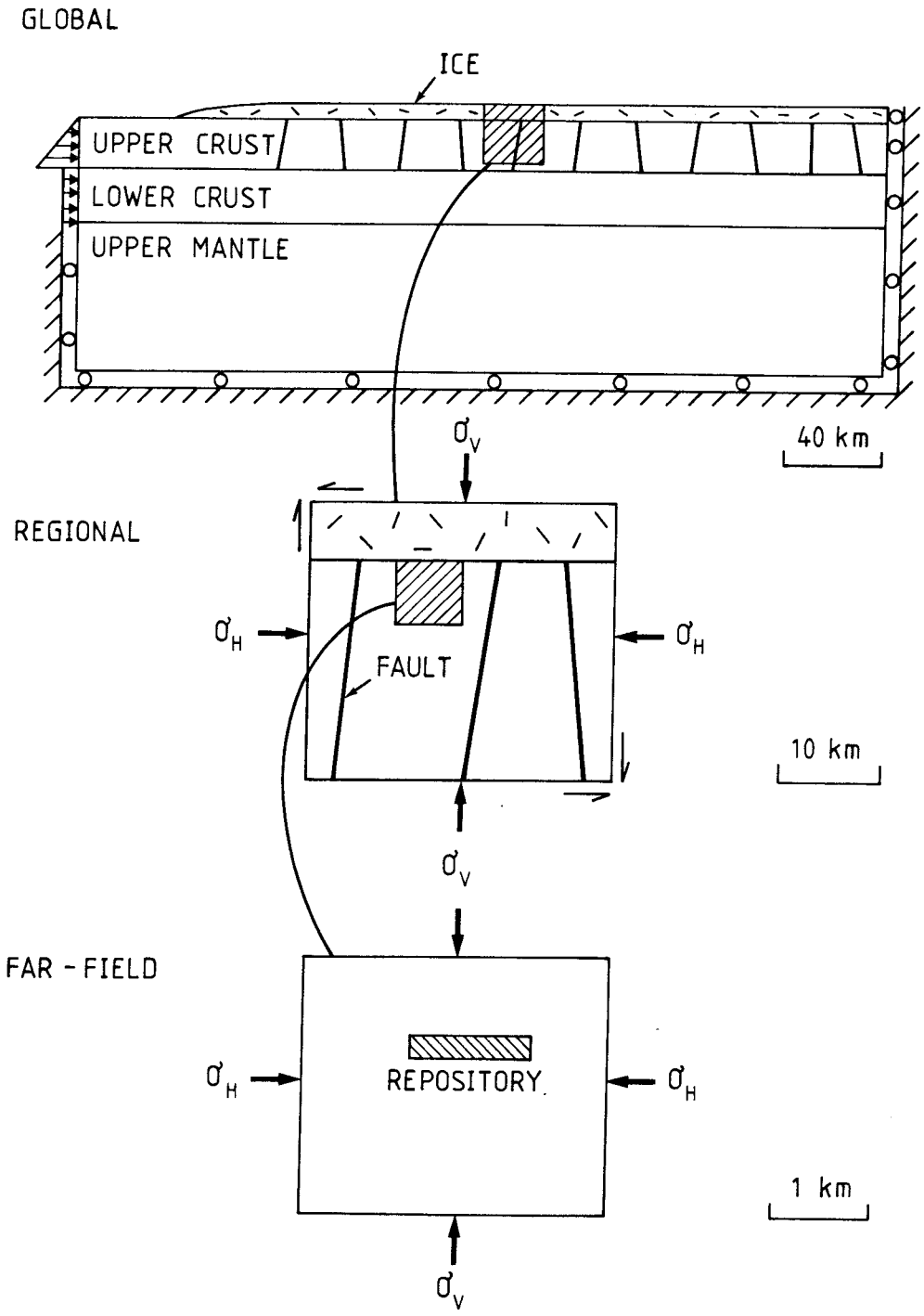


Fig. 4.6 Illustration of the scale of modelling, where a global model gives the boundary conditions for the regional and the far-field models.

# 5 STRENGTH OF GRANITIC ROCK MASSES

Rock mass behaviour, which for engineering purposes, can often be characterised by its strength, deformability and permeability, is affected by the combined behaviour of intact rock and discontinuities. Discontinuities are planar features or surfaces of smaller strength, larger deformability, and larger permeability than the intact rock.

In studies of vaults for radioactive waste disposal the rock mass discontinuity characteristics are of equal or of even greater importance in design than the much stronger and stiffer intact rock.

## 5.1 Strength of intact granitic rock

The determination of both the static and dynamic strength, under pressure, of crystalline igneous rocks in general, and granitic rocks in particular, has been the subject of numerous investigations. A number of several excellent data compilations are available, see for example, Birch (1966), Lama and Vutukuri (1978), Touloukain et al. (1981). However, very little data is available for granitic rocks, where the effects of pressure (P), temperature (T), and pore pressure ($P_o$), have been studied in one and the same experimental set up. Hence, at present, we must study these effects independently, and, in most cases, individually and subsequently evaluate the total effect.

In conventional testing, the mechanical properties of rocks are investigated by axial compression of a circular cylindrical specimen, whose length is two to three times its diameter. A stress field is applied to the cylinder. The axial and lateral strains are then measured. Stresses are plotted against strains. A stress-strain curve is then obtained. The elastic modulus and strength can then be determined. In experimental work, it is usually the case that triaxial tests are conducted with two of the applied principal stresses equal.

### 5.1.1 The effect of confining pressure

It has been known for almost a century that if the lateral displacement of a compression test specimen is resisted, by applying pressure to its sides, it becomes stronger, and there is a tendency towards increased ductility. The effect of increasing confining pressure ($\sigma_2 = \sigma_3$), for a rock sample in a stiff rock testing machine is shown in Fiugre 5.1. We see from Figure 5.1 that as the confining pressure is increased, the strength increases, and the permanent deformation before fracture also increases.

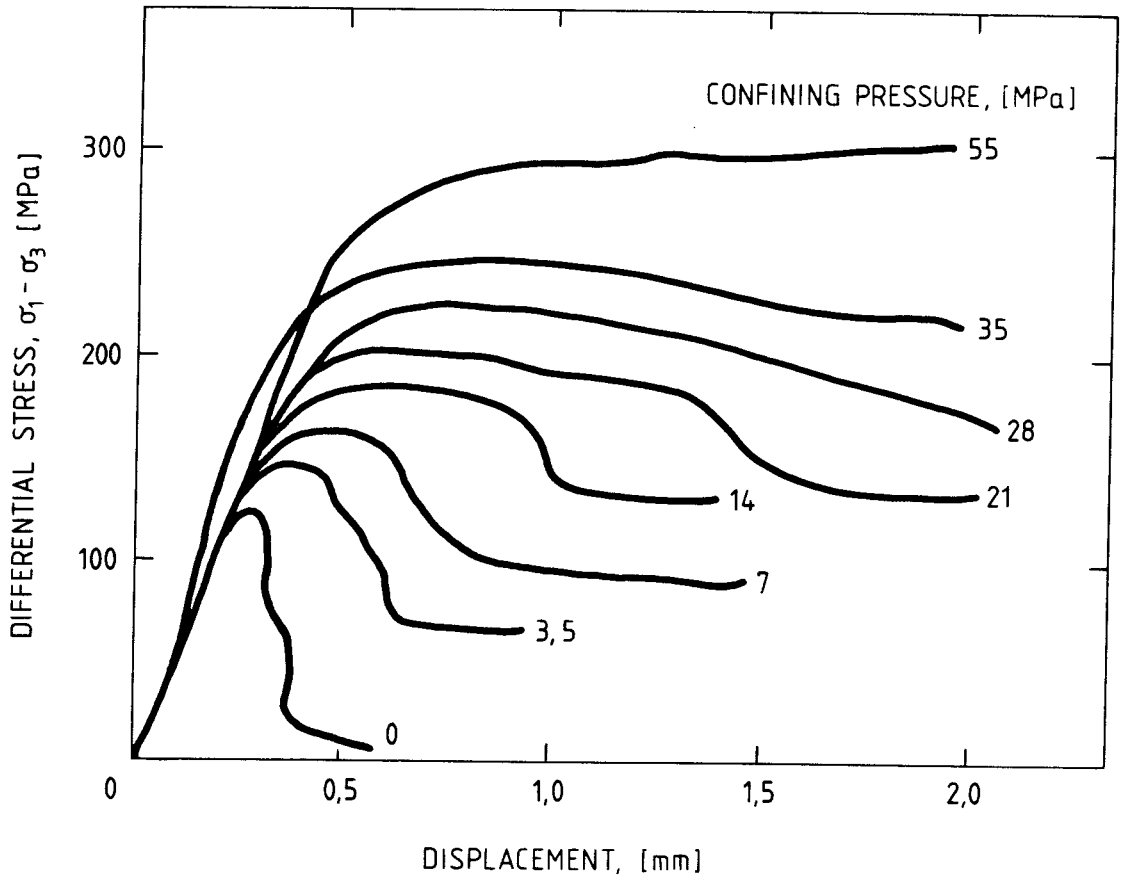


Fig. 5.1 Complete load-displacement curve for rocks in triaxial compression. After Rummel and Fairhurst (1970).

At low confining pressures, brittle fracture occurs. For most rock types, there is well-defined value of the confining pressure at which there is a transition from typicallt brittle behaviour to fully ductile behaviour. There is a clear tendency for rock material to

increase its strength with increasing confining pressure. There is also a large variation in strength for different rock types.

Figure 5.2 shows applied axial stress versus confining pressure curves for different rock types (mostly granitic). For granite, at confining stresses below 300 MPa, the increase in applied axial stress is approximately linear. Hence, in modelling the mechanical properties of the intact rock in the upper crust, the assumption of linear elastic behaviour is reasonable. Following the suggestion by Hasegawa et al. (1985) Young's moduli for the upper and lower crust are taken to be 105 GPa and 128 GPa respectively.

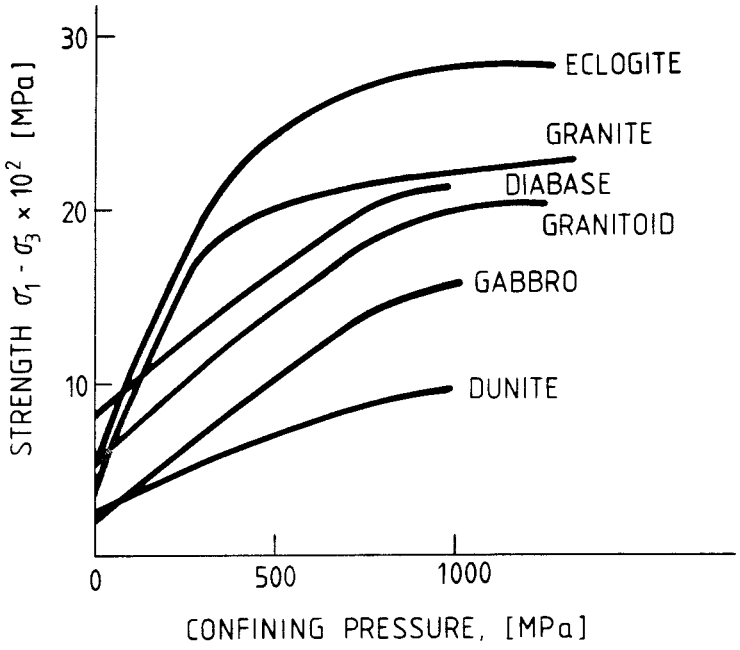


Fig. 5.2 Applied axial stress as a function of confining pressure for different rock types at room temperature. After Vutukuri et al. (1974)

For most rock types, there is a linear increase in strength with confining pressure. However, most granitic rocks show non-linear behaviour of strength versus confining pressure, for confining pressures in the range 0-260 MPa, as shown in Figure 5.3.

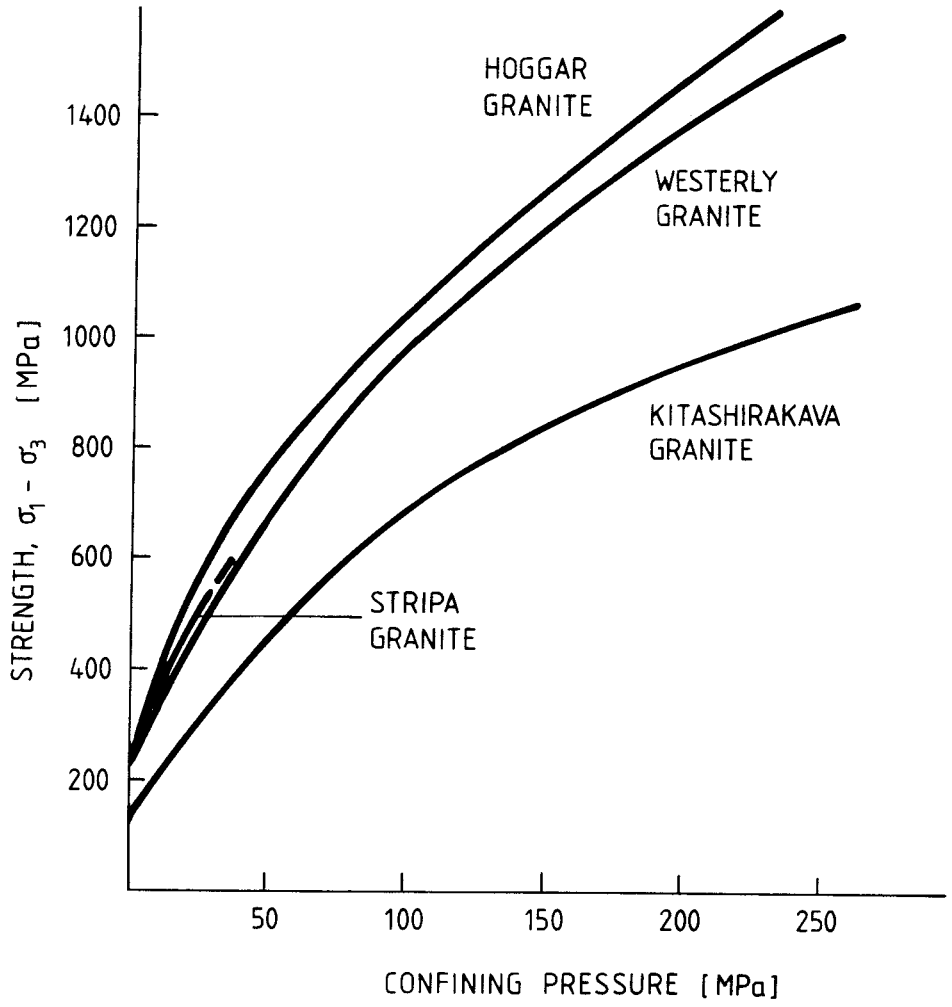


Fig. 5.3 Strength versus confining pressure for four types of granitic rocks. Data from Duba et al. (1974), Janach (1977), Matsushima (1960), Schock et al. (1972), and Swan (1978).

### 5.1.2 Influence of temperature

Although, in general, the brittle fracture of rock is relatively insensitive to changes in temperature alone, in contrast to its behaviour in the ductile regime, changes in temperature may produce quite significant effects at increased confining pressure. Failure stresses for minerals and rocks at various temperatures in triaxial compression tests are listed in several handbooks on rock properties, e.g. Birch (1966). Brittle fracture is relatively insensitive to temperature, but as the confining pressure, $\sigma_2 = \sigma_3$, increases, the effects of temperature become more important, as shown in Figure 5.4. The true effect of the influence of temperature and confining pressure for Charcoal granite is illustrated in Figure 5.5.

Here we notice a moderate decrease in strength, $\sigma_1 - \sigma_3$, as the temperature increases for both low and intermediate confining pressures.

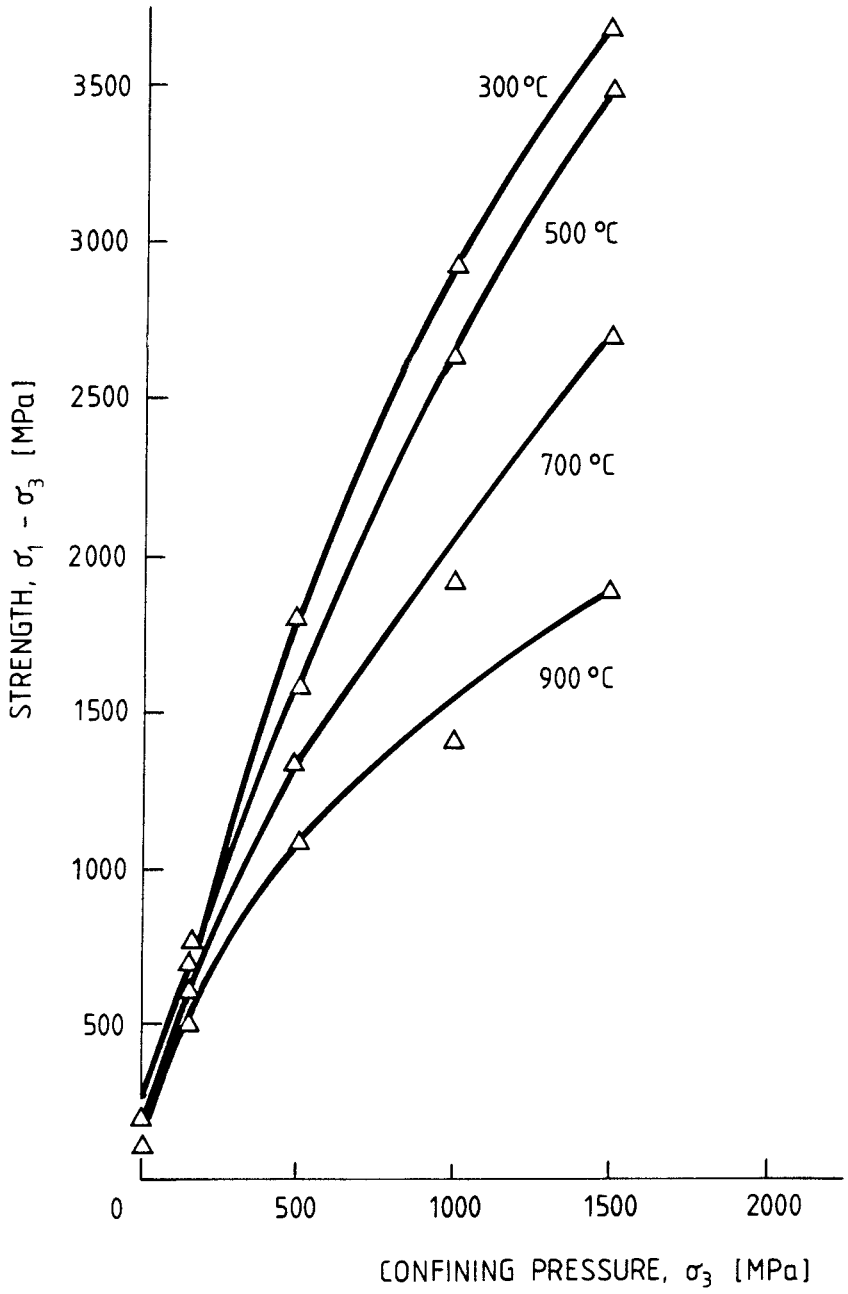


Fig. 5.4 Strength versus confining pressure for dry Westerly granite as a function of temperature. After Heuze (1983).

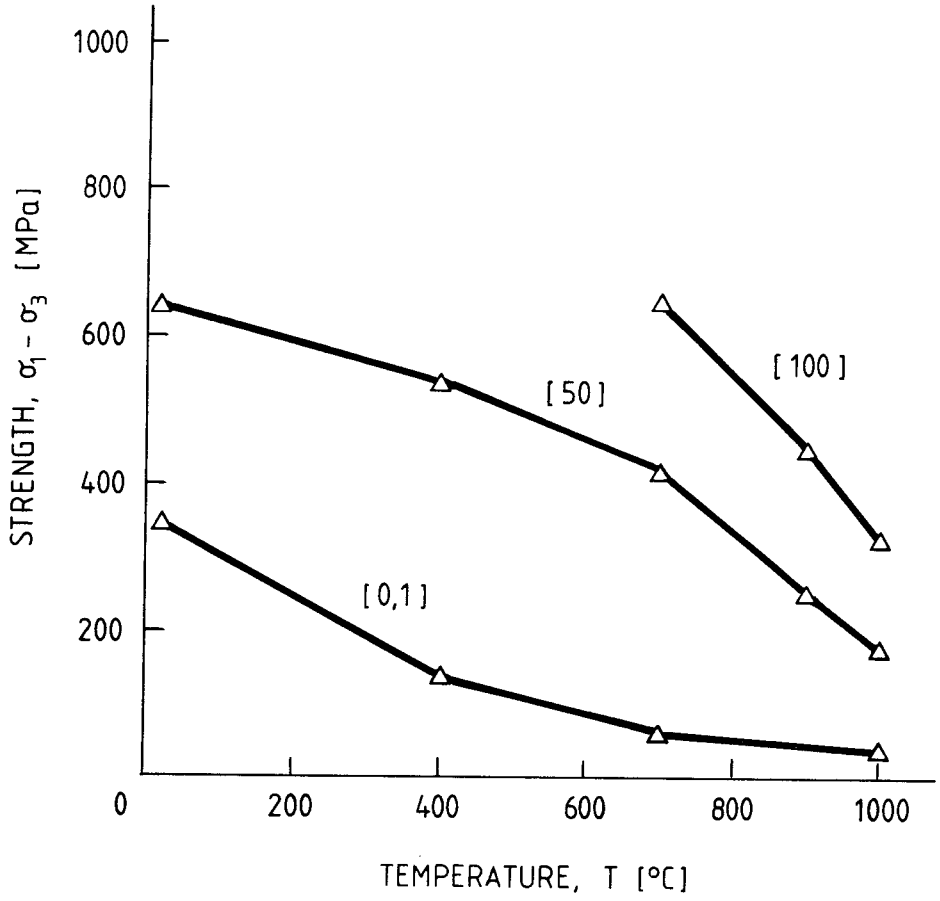


Fig. 5.5 Strength versus temperature for Charcoal granite at various confining pressures. Modified after Heuze (1983).

### 5.1.3 The effect of temperature and pressure

One important effect of increasing the temperature in rock deformation is to lower the brittle-ductile transition zone. A compilation of experimental data, where the influence of temperature and pressure are combined, allows analysis of the variation of the strength of rocks with depth in the earth's crust. Based on experimental data for Westerly granite from Rhode Island, U.S.A., reported by Clark (1966), Stetsky et al. (1974), and Tullis (1977), we can construct for this rock a strength versus depth curve, Figure 5.6. We notice how the strength increases almost linearly with depth down to about 8 km. Thereafter, the strength remains almost constant down to depths of 8-16 km. It then decreases with depth, due to the strong influence of temperature.

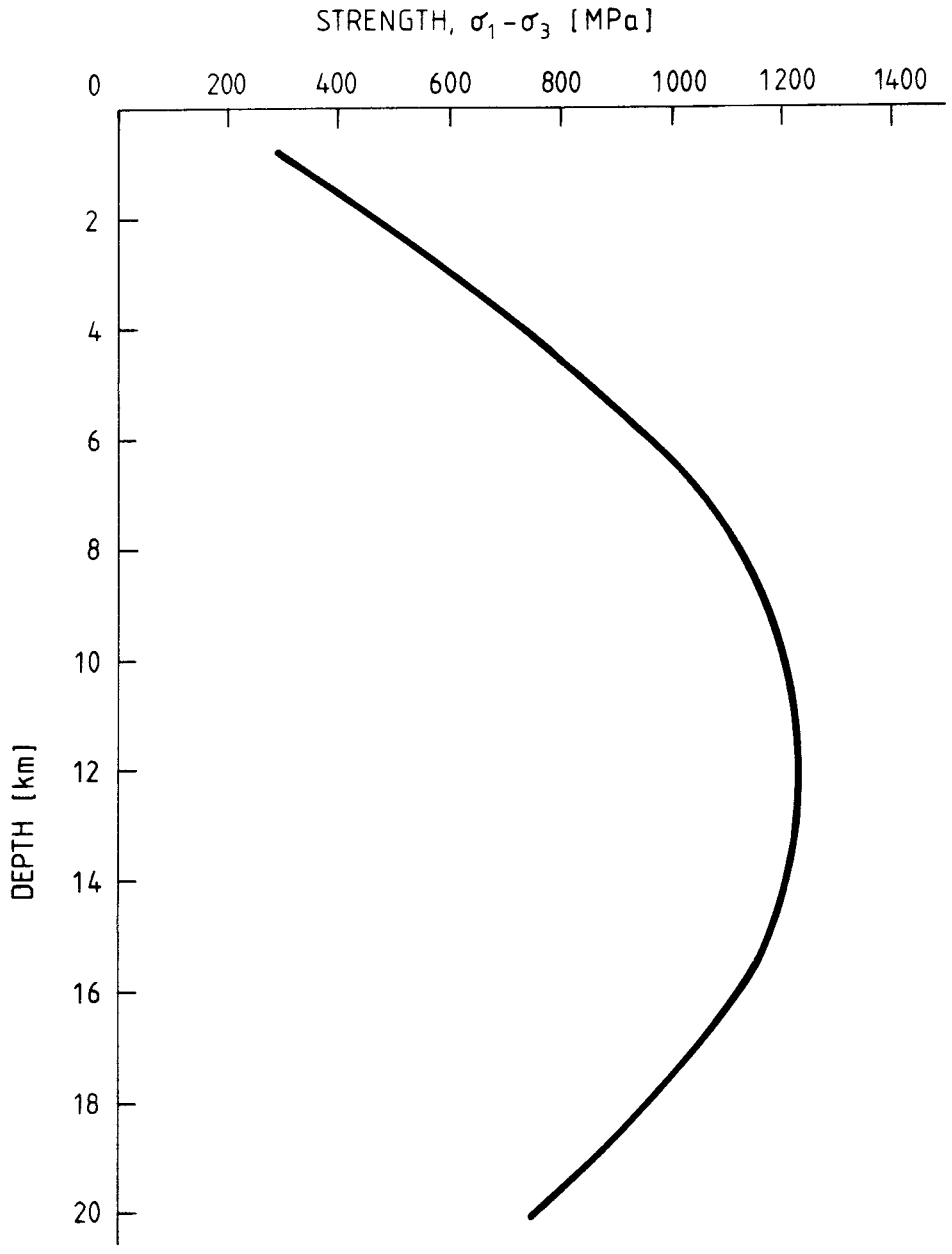


Fig. 5.6 Strength versus depth curve for Westerly granite. Data compilation from Clark (1966), Stetsky et al. (1974), and Tullis (1977).

### 5.1.4 Influence of strain rate

For a complete review of the behaviour of the strength of intact granitic rocks we must also consider the effect of strain rate. In laboratory tests on rock samples, it is most convenient to use strain rates in the range 0.001 to 0.1 millistrains per second. At these values, the strain rate is found to have a small but noticable effect on the brittle fracture stress and also on the brittle-ductile transition. In triaxial tests on igneous rocks at strain rates of $10^{-1}$ $sec^{-1}$ or higher, several authors have found increases of fracture stress of around 10 % for a $10^3$-fold increase in strain rate.

The influence of strain rate on the ultimate strength of Westerly granite for various confining pressures is shown in Figure 5.7. An increase in strain rate, $\dot{\varepsilon}$, by a factor of $10^4$ doubles the ultimate strength at a confining pressure of 100 MPa.

In modelling the crustal rock mechanics for waste disposal vaults we must consider tectonic stresses and strain rates of the order of $10^{-18}$ or less. It therefore follows that the effect of strain rate on strength can be disregarded.

## 5.2 Strength and deformability of rock discontinuities

Patton (1966) developed a model, from experimental and theoretical considerations, which is still considered to be one of the basic descriptions of discontinuity shearing. The model differentiates between mechanisms of dilational sliding "up over", and shearing through asperities, on the basis of a critical normal stress level. Following the presentation of Patton's model by H. Einstein and C. Dowding in Touloukian and Ho (1981), Figure 5.8 illustrates a set of shear force-shear deformation (u), and peak shear force ($S_p$) - normal force (N) relations, which compare shearing under different normal forces (stresses). A normal stress lower than the critical shear stresses, Test 1 in Figure 5.8, initially induces elastic deformation of an asperity up to $U_y$, the yield deformation. Sliding then follows and the joint will dilate. At a certain displacement, $U_s$, the resi-

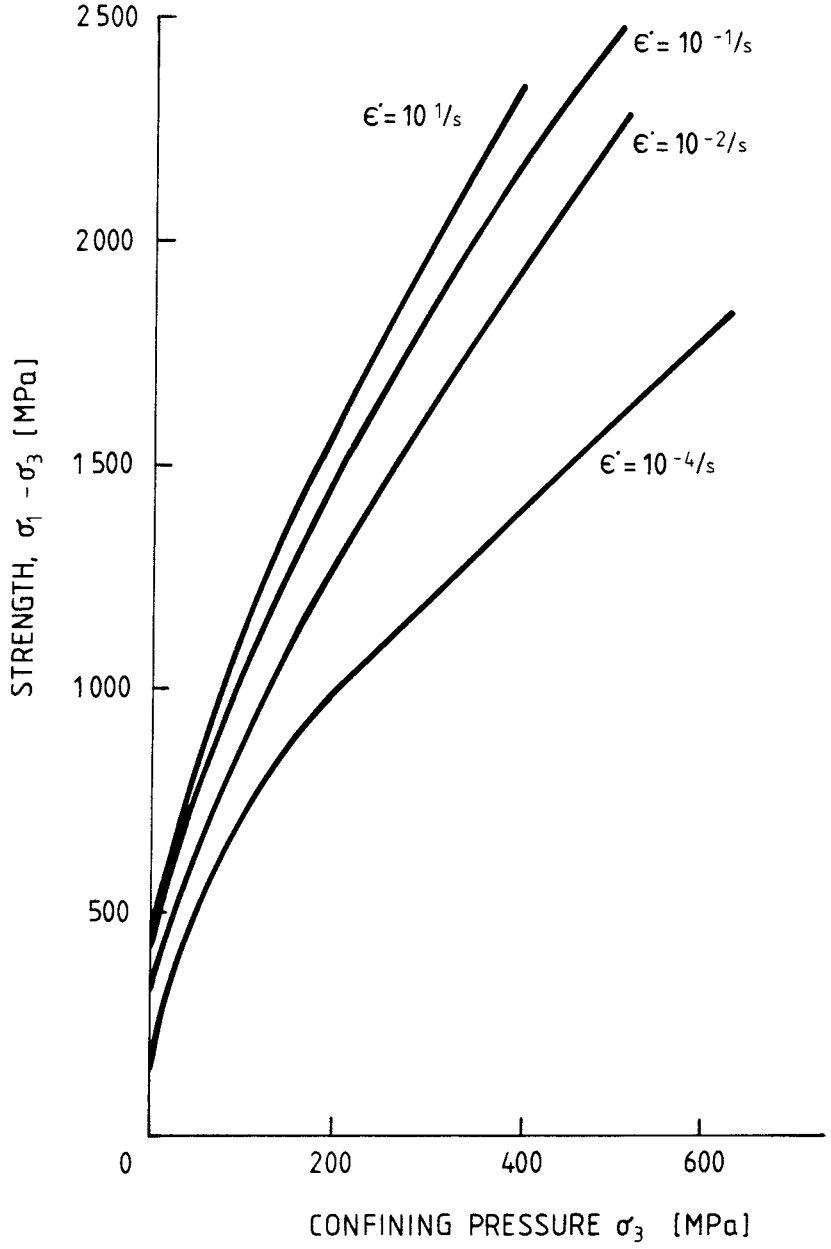


Fig. 5.7 Ultimate strength versus confining pressure and strain rate for Westerly granite.

stance of the asperity is exceeded, and shearing through the asperity occurs. Above a critical normal applied stress level (Test 2 in Figure 5.8), no dilation occurs. The asperities are then immediately sheared at their bases.

The failure envelopes in Figure 5.8 are defined as follows:

$$\tau_p = \sigma \tan (\Phi_u + i) \qquad (5.1)$$

for low normal stresses, and

$$\tau_p = c + \sigma \tan \Phi_u \qquad (5.2)$$

for high normal stresses, where:

$c$ = cohesion

$i$ = angle of asperity

$\tau_p$ = peak shear stress ($S_p/A$)

$\sigma$ = normal stress at failure (N/A)

$\Phi_u$ = angle of sliding friction

$\Phi_r$ = residual friction angle

The Coulomb criterion in equation (5.2) is probably the best known resistance curve description, since it contains a stress dependent (tan $\Phi$), and a stress independent parameter (C).

From a large number of shear tests on rocks loaded to normal stresses, $\sigma$, up to 2000 MPa, Byerlee (1978) reports the following equations for frictional shear stresses generated in rocks:

$$\tau = 0.85\sigma \qquad \text{for } 0 < \sigma < 200 \text{ (MPa)} \qquad (5.3)$$

and

$$\tau = 50 + 0.6\sigma \qquad \text{for } \sigma > 200 \text{ (MPa)} \qquad (5.4)$$

If a pore pressure, $P_o$ is present, the effective normal stress $\sigma - P_o$ is used in stead of $\sigma$, while the effective shear stress is still $\tau$.

From in-situ stress measurements made at depth in areas of active faulting, Zoback and Healy (1984) estimated the frictional strength of

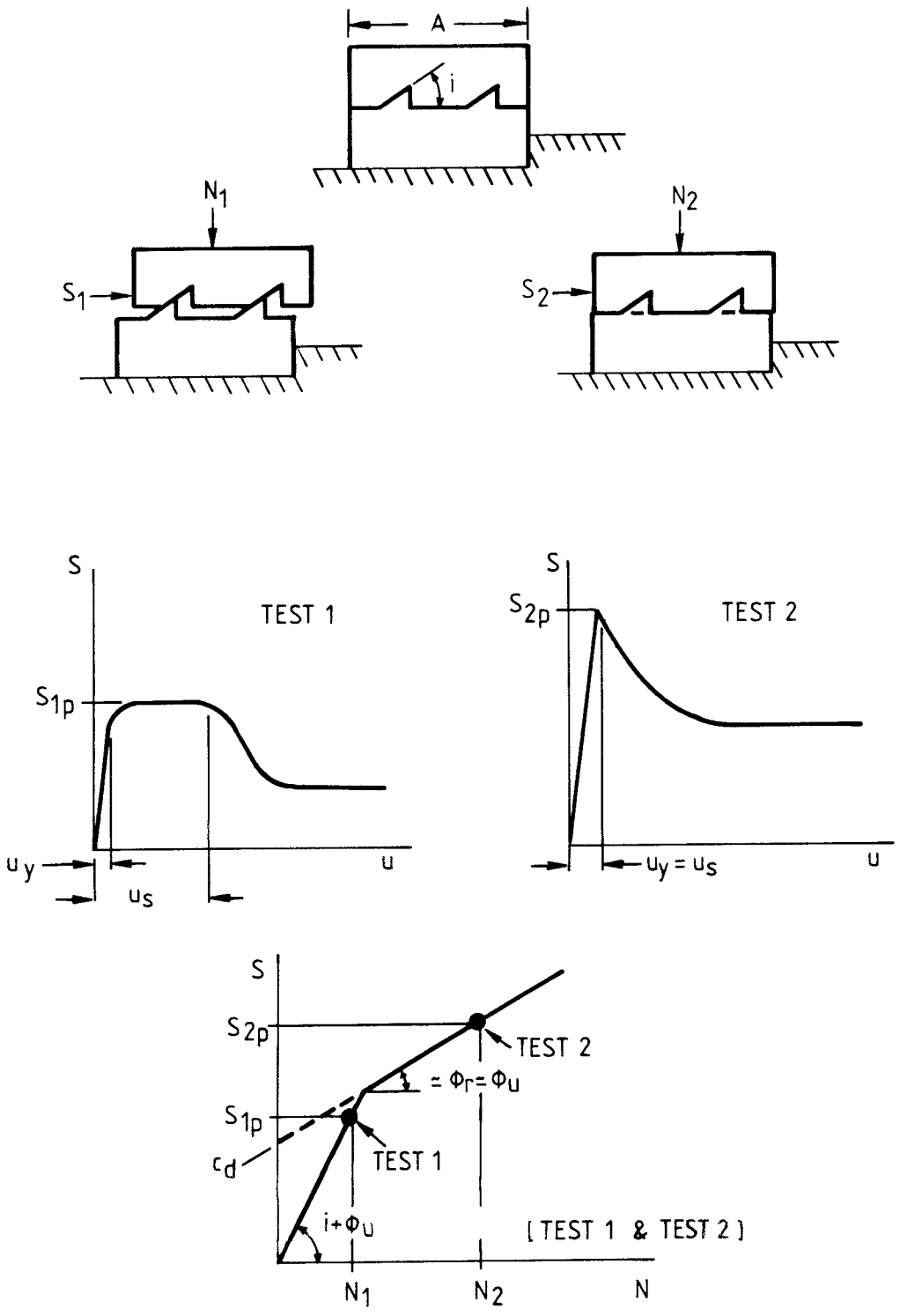


Fig. 5.8 Explanation of Patton's model for discontinuity strength. After Einstein and Dowding in Touloukian and Ho (1981).

faults at depths from 0.1 to 3.7 km. They found that the laboratory data given by equations (5.3) and (5.4) seem to apply to most faults in-situ conditions and that in areas of active faulting, the magnitude of principal stress differences in the upper crust are controlled by the frictional strength of the active faults.

Rock joints exhibit a wide range of shear strength under the low effective normal stress levels operating in most rock engineering problems. Conversely, under the high effective normal stress levels of interest to this study and the modelling of crustal rock mechanics, the range of shear strength of joints and artificial faults is small, despite the wide variation in the triaxial compressive strength of rocks at fracture. In reviewing the results of laboratory-scale tests on rock and rock joints, Barton (1977) suggested the following equation for the peak shear strength of faults through, rock up to the brittle-ductile transition

$$\tau = \sigma_n \tan (20 \log_{10} (\frac{\sigma_1 - \sigma_3}{\sigma_n}) + \Phi_b) \qquad (5.5)$$

where $\tau$ is the shear strength at a given normal stress $\sigma_n$. $\sigma_1$ and $\sigma_3$ are the major and minor principal stresses and $\Phi_b$ is the residual shear angle of friction. This empirical law formulates the friction and fracture strength and at the critical state the effective normal stress is found to be equal to the differential stress, i.e. $\sigma_n = \sigma_1 - \sigma_3$. The frictional strength of Westerly granite according to to eq. (5.5) is shown in Figure 5.9.

In modelling the frictional strength of faults for crustal rock mechanics, application of the relation given by eq. (5.5) is suggested. This is also valid for problems where the influence of pore pressure is to be studied and it has been shown to agree with the experimental results presented by Byerlee (1978).

Barton and Bandis (1982) reviewed a large body of test data to determine the influence of block size on the displacement required to mobilize peak strength. They showed that the shear strength and the

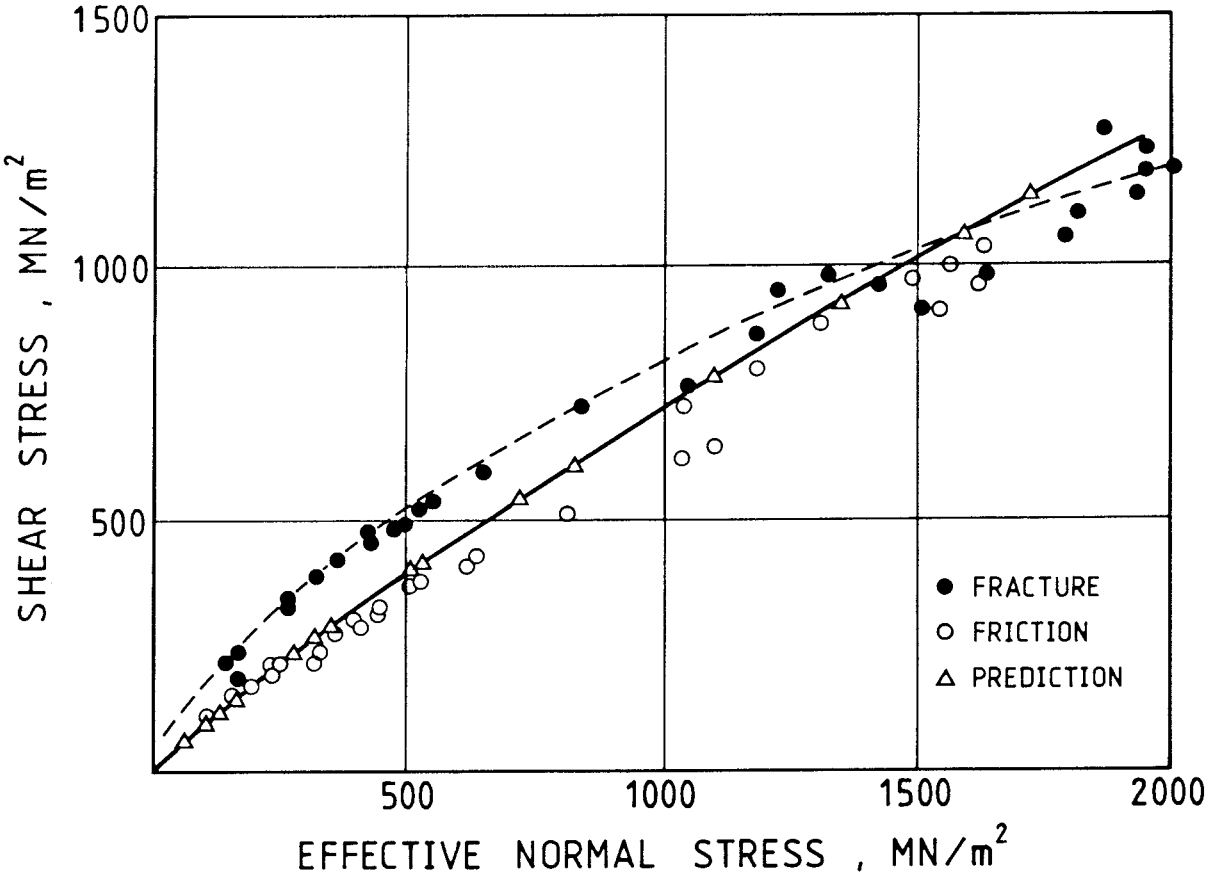


Fig. 5.9 Fracture strength, frictional strength and predicted frictional strength for Westerly granite. The predicted strength is based on eq. (5.5) with an assumed value of $\Phi_b = 30^o$. After Barton (1977).

shear stiffness are reduced with increased block size due to both reduced effective joint roughness and to reduced asperity strength. Both of these properties are a function of the delayed mobilization of roughness with increasing block size. Following the classical equation of shear strength by Barton:

$$\tau = \sigma_n \tan \left[ JRC_n \log_{10} \frac{JCS_n}{\sigma_n} + \Phi_r \right] \qquad (5.6)$$

and the suggested reductions

$$JRC_n = JRC_o \left( \frac{L_n}{L_o} \right)^{-0.02\, JRC_o} \qquad (5.7)$$

$$JCS_n = JCS_o \left( \frac{L_n}{L_o} \right)^{-0.03\, JRC_o} \qquad (5.8)$$

the shear strength can be determined for any size of joint or a fault. In the above equations,

JRC = joint roughness coefficient

JCS = joint wall compressive strength

$\sigma_n$ = effective normal stress

L = joint and fault length

$\Phi_r$ = residual friction angle of a smoothed surface

Subscripts "o" and "n" denote laboratory and natural joints/faults, respectively, see Barton and Bandis (1982). Based on shear tests on rock joints:

$JRC_o = 8.9$

$JCS_o = 92$ MPa

$\Phi_r = 27.5^o$

$L_o = 0.1$ m

These values can be substituted in equations (5.7) and (5.8). We then obtain.

$$JRC_n = 8.9 \left( \frac{L_n}{0.1} \right)^{-0.178} \qquad (5.9)$$

$$JCS_n = 92 \left( \frac{L_n}{0.1} \right)^{-0.267} \qquad (5.10)$$

Figure 5.10 shows laboratory and in-situ shear stiffness data reported in the literature. The significant effect of block size is shown and comparison is also made with the average values of stiffness derived for earthquake events. Barton and Bandis (op. cit.) also present a useful approximation to the shear stiffness in the form:

$$K_s = \frac{\sigma_n \tan \left[ JRC \log (JCS/\sigma_n) + \Phi_r \right]}{\frac{L}{500} \cdot \left( \frac{JRC}{L} \right)^{0.33}} \qquad (5.11)$$

where L is the length of the joint/fault.

A typical value of the in-situ shear stiffness for application to an upper crustal rock mechanics problem is: $K_s \approx 0.001$ MPa/mm. The normal stiffness, $K_n$, on the other hand, is probably almost independent of scale, Bandis et al. (1985).

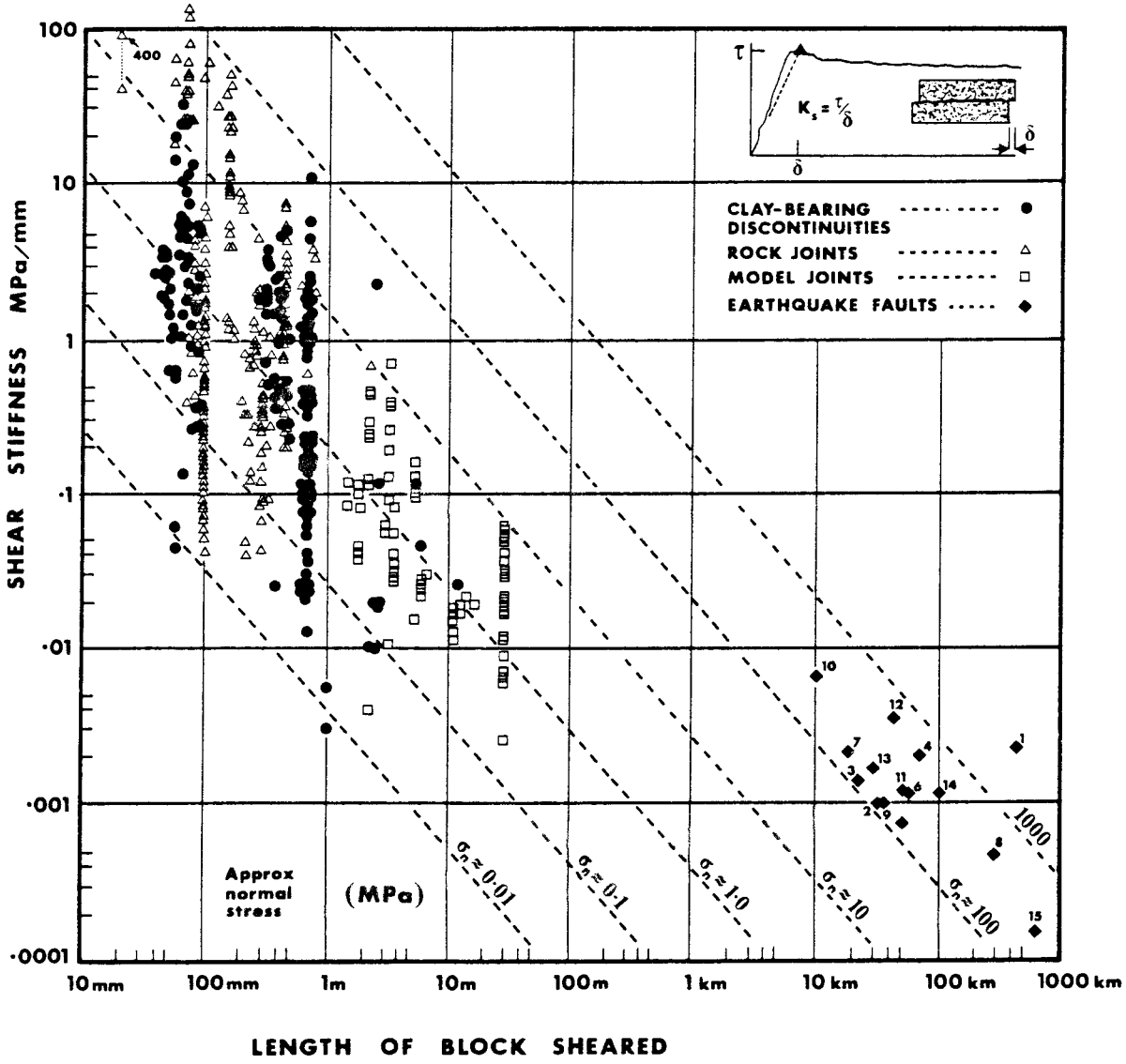


Fig. 5.10 Laboratory and in-situ shear stiffness data, reported in the literature, indicate the significant effect of block size. After Barton and Bandis (1982)

## 6 ACKNOWLEDGEMENTS

The author is grateful to Berit Alm for stimulating discussions, help in collecting basic literature, and reproducing illustrations for this report. Göran Bäckblom made valuable comments and suggestions for improvements to the first draft of the report. Comments by S. Johansson about glaciologial aspects are acknowledged. Göran Olofsson and Sonja Marklund typed the manuscript, Monica Leijon made the drawings and Peter Digby corrected the English. The author is grateful for their help.

# 7 REFERENCES

Adams, J. 1984. Glacial and postglacial stress changes in Ontario and Quebeck: Their implications for rock fracture studies. In: W.F. Heinrich (Ed) Workshop on transitional processes proceedings. Whiteshell Nuclear Research Establ., Pinawa, Manitoba. pp. 191-199.

Bakkelid, S. 1986. The determination of rates of land uplift in Norway. Tectonophysics, Vol. 130, pp. 307-326.

Bandis, S.C., Barton, N.R. and Christianson, M. 1985. Application of new numerical model of joint behaviour to rock mechanics problems. In: O. Stephansson (Ed) Proceedings of Int. Symp. on Fundamentals of Rock Joints, Björkliden, Sept. 15-20, 1985, pp. 345-355.

Barton, N.R. 1977. The shear strength of rock and rock joints. Int. J. Rock Mech. Min. Sci. & Geomech. Abstr., Vol. 13, pp. 255-279.

Barton, N.R. and Bandis, S.C. 1982. Effect of block size on the shear behaviour of jointed rock. 23rd U.S. Symposium on Rock Mechanics, Berkeley, California, pp. 739-760.

Barton, N.R. et al. 1986. Numerical analyses and laboratory tests to investigate the Ekofisk subsidence. 27th U.S. Symposium on Rock Mechanics, Univ. of Alabama, June 23-25, 1986.

Berthelsen, A. and Marker, M. 1986. 1.9 - 1.8 Ga old strike-slip megashears in the Baltic Shield, and their plate tectonic implications. Tectonophysics, Vol. 128, pp. 163-181.

Birch, F. 1966. Compressibility, elastic constants in handbook of physical constants. S.P. Clark Jr. (Ed) Memoir. Geol. Soc. Am., 97.

Bjarnason, B. and Stephansson, O. 1987. Non-linear and discontinuous stress variation with depth in the upper crust of the Baltic Shield. Proc. 6th Int. Rock Mech. Cong., Montreal, Canada. (in press)

Bott, M.H.P. and Kusznir, N.J. 1984. The origin of tectonic stress in the lithosphere. Tectonophysics, Vol. 105, pp. 1-13.

Brown, P.A., McEwen, J.H. and Rey, N. 1984. Past geological conditions and their relevance to present day fracture flow systems. In: W.F. Heinrich (Ed) Workshop on Transitional Processes Proceedings. Whiteshell Nuclear Research Establ., Pinawa, Manitoba, Canada, pp. 58-72.

Byerlee, J.D. 1967. Frictional characteristics of granite under high confining pressure. J. Geophys. Res., 72, pp. 3639-3648.

Byerlee, J.D. 1975. The fracture strength and frictional strength of Weber sandstone. Int. J. Rock Mech. Min. Sci., Vol. 12.

Bäckblom, G. 1987. Personal communication.

Duba, A.G., Heard, H.C. and Santor, M.L. 1974. Effect of fluid content on the mechanical properties of Westerly granite. Report UCRL-51626, Lawrence Livermore Laboratory, Berkeley, California.

Ekmann, M. 1985. Gaussian and mean curvatures of Earth tides and postglacial lan uplift, and their effects on earthquakes. Ph.D. Thesis, Department of Geodesy, Univ. of Uppsala, Uppsala. 87 p.

Emery, K.O. and Aubrey, D.G. 1985. Glacial rebound and relative sea levels in Europe from tide-gauge records. Tectonophysics, Vol. 120, pp. 239-255.

Eriksson, L. and Henkel, H. 1983. Deep structures in the Precambrian interpreted from magnetic and gravity maps of Scandinavia. In: Gabrielsen et al. (Eds) 4th Int. Conf. on Basement Tectonics, Oslo. pp. 351-358.

Haimson, B.C. 1982. Hydrofracturing in-situ stress measurements in the Lac du Bonnet batholith drillholes URL-1 and WN-4. Technical report prepared for Atomic Energy of Canada Ltd., Whiteshell Nuclear Research Establishment, Pinawa, Manitoba. 106 p.

Hasegawa, H.S., Adams, J. and Yamazaki, K. 1985. Upper crustal stresses and vertical stress migration in Eastern Canada. J. Geophys. Res. Vol. 90, pp.3637-3648.

Hast, N. 1958. The measurement of rock pressure in mines. Swedish Geological Survey, Ser. C, No. 560. 183 p.

Henkel, H., Hult, K., Eriksson, L. and Johansson, L. 1983. Neotectonics in Northern Sweden - geophysical investigations. Technical Report 83-57. Swedish Nuclear Fuel and Waste Management Co. (SKB), Stockholm. 64 p.

Herget, G. 1986. Changes of ground stresses with depth in the Caadian Shield. In: O. Stephansson (Ed) Proc. Int. Symp. Rock Stress and Rock Stress Measurements, Stockholm, 1-3 September, 1986. Centek Publ., Luleå. pp. 61-68.

Heuze, F.E. 1983. High temperature mechanical physical and thermal properties of granitic rocks - a review. Int. J. Rock Mech. Min. Sci. & Geomech. Abstr., Vol. 20, No. 1.

Jackson, J. and McKenzie, D. 1983. The geometrical evolution of normal fault systems. J. Struct. Geol., Vol. 5, pp. 471-482.

Janach, W. 1977. Failure of granite under compression. Int. J. Rock Mech. Min. Sci. & Geomech. Abstr., Vol. 14, pp. 209-215.

Kakkuri, J. 1986. Newest results obtained in studying the Fennoscandian land uplift phenomenon. Tectonophysics, Vol. 130, pp. 327-331.

Kelkar, S., Murphy, H. and Dash, Z. 1986. Earth stress measurements in deep granitic rock. Proc. 27th U.S. Symp. Rock Mechanics, Alabama, pp. 259-266.

Klein, R.J. and Barr, M.V. 1986. Regional state of stress in Western Europe. In: O. Stephansson (Ed) Proc. Int. Symp. Rock Stress and Rock Stress Measurements, Stockholm, 1-3 September, 1986. Centek Publ., Luleå. pp. 31-44.

Koerner, F.M. 1984. Conditions at the ice/rock interface of large ice sheets. In: W.F. Heinrich (Ed) Workshop on transitional processes, proceedings. Whiteshell Nuclear Research Establ., Pinawa, Manitoba. pp. 200-211.

Lagerbäck, R. 1979. Neotectonic structures in Northern Sweden. Geol. Fören. Stockholm Förh., Vol. 100, pp. 263-269.

Lagerbäck, R. and Witschard, F. 1983. Neotectonics in Northern Sweden - geological investigations. Technical Report 83-58. Swedish Nuclear Fuel and Waste Management Co. (SKB), Stockholm. 58 p.

Lama, R.D. and Vutukuri, V.S. 1978. Handbook on mechanical properties of rocks, Vol. II. Trans Teach Publ., Aedermannsdorf, Switzerland.

Lundqvist, J. and Lagerbäck, R. 1976. The Pärvie fault: A late-glacial fault in the Precambrian of Swedish Lapland. Geol. Fören. Stockholm Förh., Vol. 98, pp 45-51.

Martna, J., Hiltscher, R. and Ingevald, K. 1983. Geology and rock stresses in deep boreholes at Forsmark in Sweden. Proc. 5th Int. Cong. Rock Mechanics, Melbourne

Mathis, J.I. 1987. Discontinuity mapping - A comparison between line and area mapping. Proc. 6th Int. Rock Mech. Cong., Montreal, Canada. (in press)

Matsushima, S. 1960. On the deformation and fracture of granite under high confining pressure. Kyoto Tech. Univ. Disaster Prov. Res. Inst. Bull., No. 36, pp. 11-20.

Mörner, N.A. 1980. The Fennoscandian uplift: Geological data and their geodynamical implications. In: N. A. Mörner (Ed) Earth Rheology, Isostasy and Eustasy. Wiley, London. pp. 251-284.

Paterson, W.S.B. 1972. The physics of glaciers. Pergamon Press, Oxford. 250 p.

Pesonen, L.J. and Neuvonen, K.J. 1981. Paleomagnetism of the Baltic Shield - implications for Precambrian tectonics. In: A. Kröner (Ed) Precambrian Plate Tectonics. Elsevier, Amsterdam. pp. 623-648.

Pusch, R. 1986. Personal communication.

Ranalli, G. and Chandler, T.E. 1975. The stress field in the upper crust as determined from in-situ measurements. Geol. Rundschau, Vol. 64, pp. 653-674.

Salomon, S.C., Richardson, R.M. and Bergman, E.A. 1980. Tectonic stress: Models and magnitudes. J. Geophys. Res., Vol. 85, pp. 6086-6092.

Schock, R.N., Abey, A.E., Heard, H.C. and Louis, H. 1972. Mechanical properties of granite from the Taorirt Tan Afella Massif, Algeria. Report UCRL-51296, Lawrence Livermore Laboratory, Berkeley, California.

Sibson, R.H. 1983. Continental fault structure and the shallow earthquake source. J. Geol. Soc. London, Vol. 140, pp. 741-767.

Slunga, R., Norrman, P. and Glans, A-C. 1984. Baltic Shield seismicity, the result of a regional network. Geophys. Res. Letters, Vol. 11, No. 12, pp. 1247-1250.

Stephansson, O. 1983. The need of discontinuities and horizontal stresses in geological storage of radioactive waste. In: Gabrielsen et al. (Eds) Proceedings 4th Int. Conf. on Basement Tectonics, Oslo, pp 35-47

Stephansson, O. (Ed) 1986. Proceedings of the International Symposium on Rock Stress and Rock Stress Measurements, Stockholm, 1-3 September, 1986. Centek Publ., Luleå. 694 p.

Stephansson, O. and Berner, H. 1971. The finite element method in tectonic processes. Phys. Earth Planet. Interiors, Vol. 4, pp. 301-321.

Stephansson, O., Bäckblom, G., Groth, T. and Jonasson, P. 1978. Deformation of a jointed rock mass. Geol. Fören. Stockholm Förh., Vol. 100, pp. 387-394.

Stephansson, O., Särkkä, P. and Myrvang, A. 1986. State of stress in Fennoscandia. In: O. Stephansson (Ed) Proc. Int. Symp. Rock Stress and Rock Stress Measurements, Stockholm, 1-3 September, 1986. Centek Publ., Luleå. pp. 21-32.

Stephansson, O. and Ångman, P. 1986. Hydraulic fracturing stress measurements at Forsmark and Stidsvig, Sweden. Bull. Geol. Soc. Finland, Vol. 58, Part 1, pp. 307-333.

Strömberg, A.G.B. 1976. A pattern of tectonic zones in the western part of the East European Platform. Geol. Fören. Stockholm Förh., Vol. 98, pp. 227-243.

Swan, G. 1978. The mechanical properties of Stripa granite. Report LBL-7074, SAC-03, Lawrence Berkeley Laboratory, Berkeley, California.

Swedish Nuclear Fuel and Waste Management Company. 1986. Final storage of nuclear fuel. Research and Development Program 1987-1992. SKB R & D Program 86. September 1986. 84 p.

Talbot, C. 1986. A preliminary structural analysis of the pattern of post-glacial faults in Northern Sweden. TR 86-20. Swedish Nuclear Fuel and Waste Management Co. (SKB), Stockholm. 22 p.

Tirén, S. 1986. Fractures and fracture zones: Structural elements, their character and tectonic environment. A literature review. Working Report AR 86-16. Swedish Nuclear Fuel and Waste Management Co. (SKB), Stockholm. 236 p.

Touloukian, Y.S. and Ho, C.Y. 1981. Physical properties of rocks and minerals. McGraw-Hill/CINDAS Data Series on material properties, Vol. II-2. McGraw-Hill Book Co., New York.

Tullis, J. and Yund, R.A. 1977. Experimental deformation of dry Westerly granite. J. Geoph. Res., Vol. 82, No. 36, pp.5705-5718.

Vonhof, J.A. 1984. Potential hydrodynamic effects of glaciation on the Canadian Shield. In: W.F. Heinrich (Ed) Workshop on Transitional Processes Proceedings. Whiteshell Nuclear Research Establ., Pinawa, Manitoba, Canada, pp. 212-228.

Vutukuri, V.S., Lama, R.D. and Saluja, S.S. 1974. Mechanical properties of rocks, Vol. I. Trans Tech Publ., Aedermannsdorf, Switzerland.

Walcott, R.I. 1970. Isostatic response to loading of the crust in Canada. Can. J. Earth Sci., Vol. 7, pp.716-727.

Weertman, J. 1979. The unsolved general glacier sliding problem. J. Glaciology, Vol. 23, pp. 97-115.

West, G.F. 1984. Relationship between the present fracture state and the long-term (Archean to Present) tectonic and uplift history of northwest Ontario. In: W.F. Heinrich (Ed) Workshop on Transitional Processes Proceedings. Whiteshell Nuclear Research Establ., Pinawa, Manitoba, Canada, pp. 97-108.

Zoback, M.D. and Healy, J.H. 1984. Friction, faulting and in-situ stress. Annales Geophysicae, Vol. 2, pp. 689-698.

Zoback, M.L. and Zoback, M.D. 1980. State of stress in the conterminous United States. J. Geophys. Res., Vol. 85, pp. 6113-6156.

Zoback, M.L. and Zoback, M.D. 1986. Tectonic stress field in the continental U.S. In: L. Pahiser and W. Mooney (Eds) Geophysical Framework of the Continental United States. GSA Memoir. (manuscript)

# *List of SKB reports*

## Annual Reports

*1977–78*
TR 121
**KBS Technical Reports 1 – 120.**
Summaries. Stockholm, May 1979.

*1979*
TR 79–28
**The KBS Annual Report 1979.**
KBS Technical Reports 79-01 – 79-27.
Summaries. Stockholm, March 1980.

*1980*
TR 80–26
**The KBS Annual Report 1980.**
KBS Technical Reports 80-01 – 80-25.
Summaries. Stockholm, March 1981.

*1981*
TR 81–17
**The KBS Annual Report 1981.**
KBS Technical Reports 81-01 – 81-16.
Summaries. Stockholm, April 1982.

*1982*
TR 82–28
**The KBS Annual Report 1982.**
KBS Technical Reports 82-01 – 82-27.
Summaries. Stockholm, July 1983.

*1983*
TR 83–77
**The KBS Annual Report 1983.**
KBS Technical Reports 83-01 – 83-76
Summaries. Stockholm, June 1984.

*1984*
TR 85–01
**Annual Research and Development Report 1984**
Including Summaries of Technical Reports Issued during 1984. (Technical Reports 84-01– 84-19)
Stockholm June 1985.

*1985*
TR 85-20
**Annual Research and Development Report 1985**
Including Summaries of Technical Reports Issued during 1985. (Technical Reports 85-01-85-19)
Stockholm May 1986.

*1986*
TR86-31
**SKB Annual Report 1986**
Including Summaries of Technical Reports Issued during 1986
Stockholm, May 1987

## Technical Reports

*1987*
TR 87-01
**Radar measurements performed at the Klipperås study site**
Seje Carlsten, Olle Olsson, Stefan Sehlstedt, Leif Stenberg
Swedish Geological Co, Uppsala/Luleå
February 1987

TR 87-02
**Fuel rod D07/B15 from Ringhals 2 PWR: Source material for corrosion/leach tests in groundwater**
**Fuel rod/pellet characterization program part one**
Roy Forsyth
Studsvik Energiteknik AB, Nyköping
March 1987

TR 87-03
**Calculations on HYDROCOIN level 1 using the GWHRT flow model**
**Case 1 Transient flow of water from a borehole penetrating a confined aquifer**
**Case 3 Saturated-unsaturated flow through a layered sequence of sedimentary rocks**
**Case 4 Transient thermal convection in a saturated medium**
Roger Thunvik, Royal Institute of Technology, Stockholm
March 1987

TR 87-04
**Calculations on HYDROCOIN level 2, case 1 using the GWHRT flow model**
**Thermal convection and conduction around a field heat transfer experiment**
Roger Thunvik
Royal Institute of Technology, Stockholm
March 1987

TR 87-05
**Applications of stochastic models to solute transport in fractured rocks**
Lynn W Gelhar
Massachusetts Institute of Technology
January 1987

TR 87-06
**Some properties of a channeling model of fracture flow**
Y W Tsang, C F Tsang, I Neretnieks
Royal Institute of Technology, Stockholm
December 1986

TR 87-07
**Deep groundwater chemistry**
Peter Wikberg, Karin Axelsen, Folke Fredlund
Royal Institute of Technology, Stockholm
June 1987

TR 87-08
**An approach for evaluating the general and localized corrosion of carbon steel containers for nuclear waste disposal**
GP March, KJ Taylor, SM Sharland, PW Tasker
Harwell Laboratory, Oxfordshire
June 1987

TR 87-09
**Piping and erosion phenomena in soft clay gels**
Roland Pusch, Mikael Erlström,
Lennart Börgesson
Swedish Geological Co, Lund
May 1987

TR 87-10
**Outline of models of water and gas flow through smectite clay buffers**
Roland Pusch, Harald Hökmark,
Lennart Börgesson
Swedish Geological Co, Lund
June 1987